UNIVERSITÉ DE MONTRÉAL

REAL-TIME INTRAOPERATIVE SPECTROSCOPIC MARGIN DETECTION IN ROBOTIC-ASSISTED RADICAL PROSTATECTOMY ON PROSTATE CANCER PATIENTS

MICHAEL PINTO

INSTITUT DE GÉNIE BIOMÉDICAL

ÉCOLE POLYTECHNIQUE DE MONTRÉAL

MÉMOIRE PRÉSENTÉ EN VUE DE L'OBTENTION

DU DIPLÔME DE MAÎTRISE ÈS SCIENCES APPLIQUÉES

(GÉNIE BIOMÉDICAL)

AOÛT 2018

UNIVERSITÉ DE MONTRÉAL

ÉCOLE POLYTECHNIQUE DE MONTRÉAL

Ce mémoire intitulé :

REAL-TIME INTRAOPERATIVE SPECTROSCOPIC MARGIN DETECTION IN ROBOTIC-ASSISTED RADICAL PROSTATECTOMY ON PROSTATE CANCER PATIENTS

présenté par : PINTO Michael

en vue de l'obtention du diplôme de : Maîtrise ès sciences appliquées

a été dûment accepté par le jury d'examen constitué de :

M. STIKOV Nikola, Ph. D., président

M. LESAGE Frédéric, Ph. D., membre et directeur de recherche

Mme TRUDEL Dominique, Ph. D., membre et codirectrice de recherche

M. RAISON Maxime, Ph. D., membre

DEDICATION

To the men who selflessly consented to this research and for those it may one day benefit.

ACKNOWLEDGEMENTS

As the adage goes: it takes a village to raise a master's student.

First and foremost, a huge thank you to my parents who've been behind me every step of the way - your love, support and devotion to education have brought me where I am today and for that I could not be more grateful.

Thank you to my academic supervisors, Frederic Lesage and Dominique Trudel for constantly pushing me to research further, challenge my ideas and achieve my ambitions. Your passion and dedication to your research are as palpable as they are contagious.

Thank you to Frederic Leblond for bringing forth this project and showing by example what it means to be an innovator. Every meeting, phone call, and e-mail with you tapped into a stream of new ideas in a way that will leave me inspired for years to come.

Thank you to Kevin Zorn for your excitement in collaborating on this project and for taking precious time out of your surgeries to make it a reality.

A big thanks to the industrial partners behind this research and more importantly the people that helped along every step of the way. Thank you to Ian McDowall for your invaluable advice and for the warm welcome at Intuitive headquarters, to Rajeev Yadav for technical guidance and brainstorming sessions and to Chris Kent for trusting me with this research and coaching me along the way. Thank you also to Diane Coté and Christiane Barette at the MEDTEQ institute for your help in making this project a reality.

A heartfelt thank you to Joannie Desroches for introducing me to the world of medical optics. The past few years have been an unforgettable adventure in large part thanks to you.

This section would be incomplete without mentioning Jean-Philippe Tremblay. Thank you for your contagious love of tinkering and thank you for being such a dependable, supportive and amazing friend.

Thanks to all those at Polytechnique and the CHUM who contributed to this project. Mirela Birlea and Claudia Zyed, thank you for recruiting patients and providing invaluable support and thanks to Kelly Aubertin for showing me the ropes.

Finally, a warm thank you to my girlfriend Jackie for being so supportive and helping me keep my head up every step of the way. You made it easy to keep going even when I saw no end in sight.

RÉSUMÉ

Le cancer de la prostate est souvent traité par la résection de la prostate entière, une procédure appelée prostatectomie radicale. Le succès de cette procédure dépend de la capacité du chirurgien a retirer la totalité de la prostate et à assurer qu'il ne reste aucunes cellules cancéreuses à la marge chirurgicale. On retrouve du cancer à la marge dans jusqu'à 20% des procédures et à ce jour, les marges ne sont évaluées par un pathologiste que plusieurs heures après la chirurgie nécessitant des traitements adjuvants quand du cancer est détecté. La capacité de caractériser du tissue de façon intra opératoire et en temps réel est donc un réel besoin clinique qui n'est pas comblé par la technologie actuelle. La spectroscopie Raman est une technologie optique basée sur la diffusion de la lumière par des molécules et liens moléculaires spécifiques. La spécificité moléculaire de la spectroscopie Raman peut être couplée à des techniques d'apprentissage machine pour effectuer de la caractérisation de tissu en fonction de sa composition moléculaire. Ceci pourrait combler le besoin clinique énoncé en permettant aux chirurgiens de détecter et retirer le maximum de tissu prostatique bénin et cancéreux. Dans ce mémoire, nous présentons la conception et le développement d'un système de spectroscopie Raman intégré à une plateforme de chirurgie robotisée couramment utilisée pour effectuer des prostatectomies. L'ingénierie du système et sa validation sur des fantômes sont d'abord présentés. Nous présentons ensuite une preuve de concept effectuée sur 20 prostates humaines *ex vivo* pour démontrer la capacité du système à distinguer entre du tissu de prostate et du tissu extra-prostatique avec une précision, sensibilité et spécificité tous au-delà de 90%. Finalement, nous présentons l'utilisation du système avec une plateforme de chirurgie robotisée pour effectuer, pour la première fois, des mesures de spectroscopie Raman *in vivo* sur des prostates humaines pendant la prostatectomie.

ABSTRACT

Prostate cancer is often treated through a radical prostatectomy procedure consisting of the removal of the entirety of the prostate gland. The success of this procedure relies on the surgeon's ability to resect prostate tissue maximally and ensure no cancer is left behind. Surgical margins are currently assessed by pathologists only hours to days following surgery and positive surgical margins (cancer cells having spread to the boundary of resection) occur in as many as 1 in 5 cases. The ability to characterize tissue intraoperatively, in real time is therefore an important clinical need and is unmet by current technology. Raman spectroscopy (RS) is an optical technology based on the scattering of light by specific molecules/molecular bonds. Combining the molecular specificity of RS with machine learning techniques has shown promise for tissue characterization based on molecular composition. This sort of molecular fingerprinting could benefit prostatectomy procedures by ensuring maximal resection of prostate tissue and cancer. In this thesis, we present the design and development of an RS system integrated to a surgical robotics platform commonly used in RP. Design, engineering, and validation work on phantoms is presented. A proof of concept study was performed to demonstrate the ability of RS to characterize prostate tissue wherein the system was used to obtain data on 20 whole human prostates *ex vivo.* Preliminary results show successful distinction between prostatic and extra-prostatic tissue with accuracy, sensitivity and specificity over 90%. Also presented is the successful use of the system with a surgical robot to perform *in vivo* measurements in humans on 5 patients for the first time.

TABLE OF CONTENTS

LIST OF TABLES

LIST OF FIGURES

LIST OF SYMBOLS AND ABBREVIATIONS

CCD	Charge coupled device
FP	Fingerprint
H&E	Hematoxylin & Eosin
HWN	High wavenumber
LDA	Linear discriminant analysis
LRP	Laparoscopic radical prostatectomy
MTP	Mechanical transfer push-on
ORP	Open radical prostatectomy
PCA	Principal component analysis
RARP	Robotic assisted radical prostatectomy
RS	Raman spectroscopy
SNV	Calmodulin
SVM	Support vector machine

CHAPTER 1 INTRODUCTION

1.1 Prostate Cancer, treatment, and clinical motivation

Prostate cancer occurs when cells from the prostate gland begin to grow uncontrollably. It is the second most frequently diagnosed cancer globally[1] . In the United States in 2015 there were an estimated 220,800 new prostate cancer cases (26% of all 2015 cases) and 27,540 deaths (9% of all 2015 estimated cancer deaths)[2] .

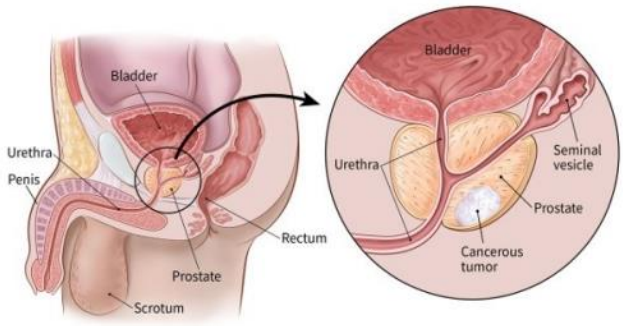

Figure 2.1 : Human reproductive anatomy with closeup view of prostate and prostate cancer. Source : https://www.cancer.org/cancer/prostate-cancer/about/what-is-prostate-cancer.html

Surgical excision of the whole prostate through Radical Prostatectomy (RP) is an important standard of care for prostate cancer and can be performed through open (ORP), laparoscopic (LRP) or robotic assisted (RA-RP) surgical methods. Minimally invasive techniques such as LRP and RA-RP have comparable clinical outcomes to ORP. However, RA-RP leads to shorter catheterization times and hospital stays, less blood loss and reduced complication rates[3]. Moreover, the robots used for RA-RP offer a platform well suited for the integration and control of assistive technologies with minimal perturbation to the surgeon's workflow.

The clinical objective of the procedure is to remove the entire prostate while sparing nerves and other surrounding tissues. This presents surgeons with several clinical challenges unmet by present technology. Firstly, removing the whole organ is made difficult by the lack of clear histological prostate capsule leading to prostate tissue left behind in as many as 29% of cases[4]. Moreover, positive surgical margins (cancer cells having spread into surrounding marginal tissue) occur in as

many as 1 in 5 cases and strongly correlate with disease recurrence[5]. Positive surgical margins are only discovered following surgery, when pathologists study the excised prostate. Finally, detection of nerves vital to erectile and urinary function could lead to more effective nerve sparing which has important impacts on post-operative erectile function and urinary continence[6]. As such, there is an important clinical need for a real time, in vivo method to characterize tissue during RP to insure more complete resections, detect cancer at the margin and lead to better outcomes with regards to urinary continence and erectile disfunction.

1.2 Raman spectroscopy for tissue characterization

Raman spectroscopy (RS) is an optical technology that has shown promising results for sensitive and specific molecular characterization of tissue[7][8]. RS is based on the detection of inelastically scattered light following tissue excitation with monochromatic light[9]. When light is incident on tissue, the most probable interaction process is elastic scattering (Rayleigh scattering) resulting in light reemission at the same frequency as the excitation. The Raman effect is associated with a small fraction of the reemitted light instead being scattered at a frequency different from that of the incident photons. The resulting spectral shifts are associated with molecular vibrations and provide an avenue for precise and quantitative fingerprinting since each molecular species have their own spectral signature. A more detailed overview of Raman spectroscopy and its clinical applications is presented in section 2 of this thesis.

Previous work performed using RS shows great promise for its use as a diagnostic tool. For example RS has been shown to detect high grade glioblastoma (brain cancer) *in vivo* during surgery where it successfully differentiated normal brain from cancer tissue in 17 patients with grade 2-4 gliomas with a sensitivity of 93% and a specificity of 91% (as compared to standard H&E analysis)[10]. More specific to prostate cancer, RS has been shown to identify prostate cancer with high accuracy *in vitro* and *ex vivo* (see section 2.3 for a detailed review on the subject) though, to our knowledge, no studies have performed *in vivo* RS characterization of prostate tissue.

1.3 Research objectives

The general objective of this thesis is to demonstrate that a RS can be integrated into the da Vinci surgical platform for RA-RP to collect RS spectra at the surgical margin during RA-RP with the aim of characterizing tissue composition. An emphasis is placed on the engineering and integration work required to integrate RS with RA-RP and preliminary results on both *ex vivo* and *in vivo* datasets gathered using this system are presented. The central hypothesis supporting this work is that RS could be used during RA-RP and has potential for prostate tissue characterization/classification. To test this hypothesis, the objectives of this research project are listed below :

Objective 1: Integrate RS into the da Vinci surgical robotics platform

Objective 1.1 : Perform hardware and software engineering necessary for robotic integration of RS to the da Vinci surgical platform

Objective 1.2 : Verify and validate integration using a phantom of known molecular composition and geometry

Objective 2: Collect *ex vivo* and *in vivo* Raman spectra from human prostate and peri prostatic organs/tissues

Objective 2.1 : Collect Raman spectra from whole, unprocessed prostates immediately following RP with the objective characterising Raman spectra in different prostatic regions

Objective 2.2 : Collect Raman spectra from prostate and peri-prostatic organs *in vivo* to assess the feasibility of distinguishing between prostatic and peri-prostatic tissue intra operatively

Objective 2.3 : Automate the process of acquiring Raman spectra from cross sectional prostate slices following RP with the objective of distinguishing between benign and malignant prostatic tissue in a manner that is independent of the heterogeneous molecular background associated with the prostate.

Objective 3: Classify and characterize tissue based on acquired datasets

Objective 3.1 : Train algorithms capable of differentiating prostatic from peri-prostatic tissue

Objective 3.2 : Compare *ex vivo* and *in vivo* spectra

CHAPTER 2 BACKGROUND THEORY & LITERATURE REVIEW

2.1 Raman Scattering & the Raman spectrum

Light (photons) incident on a sample (be it solid, liquid, or gas) will be scattered by atoms or molecules which make up the medium and are of much smaller size than the light source wavelength. The electric field from an incident photon induces oscillating polarizations in the molecular bonds of the medium, bringing the molecules to a virtual energy state higher than its permitted vibrational states. This virtual energy state can then interact with the molecules permitted vibrational states. The first (and most likely) type of interaction is for the molecules to return to their original state (the most probable being the ground state) emitting a photon with the same frequency and wavelength as the light source. This phenomenon is referred to as elastic scattering (also referred to as Rayleigh scattering)[11]. Another form of scattering, inelastic or Raman scattering was first postulated by Smekal in 1923[9] and observed experimentally in 1928[12] by Indian scientist C.V Raman and his student K. S Krishnann. They observed that when a sample is excited with a light source of a given wavelength, a much weaker spectrum composed of peaks of light of wavelengths higher and lower than the excitation wavelength is emitted. These emissions are the result of interactions between a virtual energy state and vibrational energy states different from the one the molecule was in when it encountered the photon. The molecule ends in a vibrational state higher or lower than the one it was in before interaction (either absorbing energy or transferring some in the process) and a photon of either higher or lower wavelength than the incident one is emitted. This process is known as inelastic scattering (also referred to as Raman scattering). A molecule that is left in a higher vibrational state will scatter a photon with lower energy (referred to as Stokes Raman scattering) than the incident one and one in which the molecule is left in a lower vibrational state than it began in will scatter a photon with higher energy (referred to as anti-Stokes Raman scattering) than the incident one. Since molecules are far more probable to be in lower vibrational states when they scatter a photon, Stokes Raman scattering is more intense than its anti Stokes counterpart and will be the focus of this work.

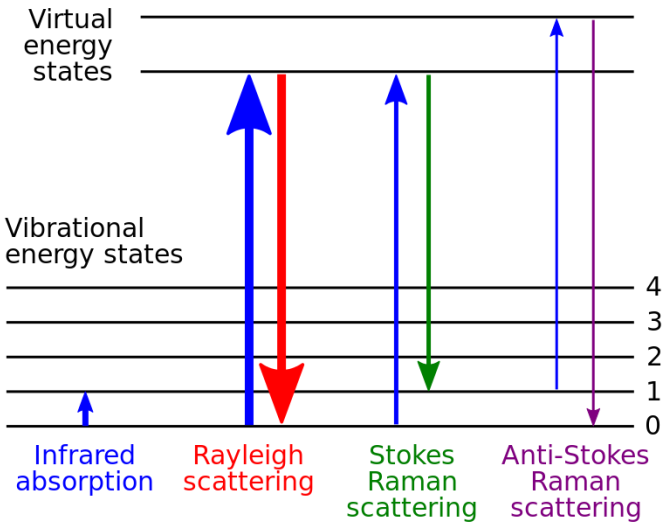

Figure 2.1 : Visual depiction of possible interactions between vibrational and virtual energy states following excitation with monochromatic light. Source : https://commons.wikimedia.org/wiki/File:Raman_energy_levels.svg

The different molecules and molecular bonds that make up a sample excited by monochromatic light will each have different vibrational/virtual energy states and will therefore result in the emission of photons of distinct wavelengths around the excitation one. Using a spectrometer and specialized equipment to collect this light, it is possible to record the spectrum of light emitted by an excited sample: the Raman spectrum. Since Raman scattering is so deeply related to the molecular make-up of the scattering material, the spectrum of light generated can be used as a sort of molecular fingerprint: this is the basis of Raman spectroscopy. Raman spectra are typically expressed in terms of shifts from the excitation wavelength (Raman shifts) and have units of wavenumbers since the spectrum is independent of excitation wavelength. The spectral range of Raman shifts from 400 – 1800 cm^{-1} is typically referred to as the “Fingerprint” (FP) region while the range of Raman shifts from 2000-3000 cm^{-1} is commonly referred to as the “high-wavenumber” (HWN) region. Figure 3 shows the Raman spectrum for a sample of acetaminophen (more commonly known as Tylenol) :

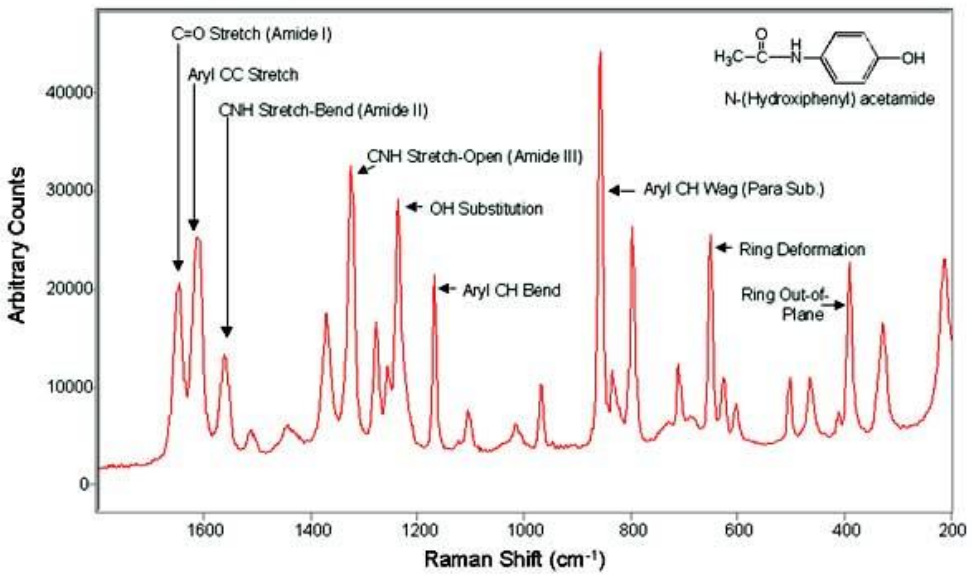

Figure 2.2 : Typical acetaminophen (Tylenol) Raman spectrum in the FP region. Acetaminophen is commonly used as a reference in literature. Source : https://commons.wikimedia.org/wiki/File:Acetominophen_Raman.jpg

It is worth noting that Raman scattering is a very rare effect (approximately 1 in 10^6 photons) that is in direct competition with other interactions between light and samples. Most notably for Raman spectroscopy of biological samples, the Raman spectrum is several orders of magnitude smaller than auto-fluorescence caused by the interaction between fluorophores present in the sample and light[13].

Raman spectroscopy systems share the same core components: a monochromatic excitation source, an optical device which delivers the excitation light to the sample and collects the spectral response, a high throughput spectrometer and a highly sensitive CCD detector to digitize the spectral response[14]. Recent technological advances in each of these components allows the development of systems which are compatible with clinical use. Notably, wavelength stabilized monochromatic lasers, high throughput and resolution spectrometers and highly sensitive CCD detectors have allowed the collection of a Raman spectrum at reasonable time scales (a couple of seconds)[15]. Moreover, advances in fiber optic light delivery/collection and miniaturized optical elements/filters have allowed the development probes which are capable of delivering excitation light and

collecting a spectral signature while filtering out the predominant Rayleigh scattering from excitation. The use of fiber optics and miniature filters has allowed the development of probes which can deliver/collect light several meters from the excitation source/detector making them suitable as handheld probes in a sterile surgical field.

2.2 Spectral processing and classification

Collecting spectra is not enough for effective use of RS as a clinical tool. Spectra need to be analyzed and transformed into easily interpretable and clinically relevant information. Uncovering the subtle molecular differences that mark the difference between, for example, spectra from healthy and diseased tissue, requires a large dataset of properly processed and labeled spectra. The first step to gathering a dataset is to determine appropriate strategy to establish ground truth in labels. There should be an observable molecular difference that exists between classes and a way to ensure it is properly labeled across spectra. For example, analysis of samples interrogated can be performed by a histopathologist to provide ground truth in distinguishing between spectra from benign and malignant tumors, cell lines of known origins can be cultured and measured, spectra can be acquired from specific anatomical structure, etc. It is worth noting that the accuracy of the method chosen in labeling for ground truth poses a limitation on the accuracy of any following classification methods. Once ground truth is established, the use of automated machine learning approaches requires sufficiently large datasets to perform blinded validation and avoid over-fitting of the data (at least 75-100 spectra to test a “good but not perfect” classifier according to a recent study from Cornell university[16]). This is often an important hurdle in clinical applications where obtaining large quantities of spectra can be complicated, lengthy and costly. With a large labeled dataset, it is then important to perform appropriate spectral processing and normalization. Common preprocessing steps of Raman spectra exist for comparison of spectra across datasets (e.g across patients). These include noise reduction using smoothing filters or frequency-based analysis, auto-fluorescence background removal to separate the Raman spectrum from excitation induced tissue auto-fluorescence[13][17], subtraction of an excitation free spectral acquisition to correct for ambient lighting, cosmic ray detection, normalization to compare spectra across datasets[18], and instrument response correction/calibration using a known standard[19] to compare datasets across

systems. Many different techniques exist for each one of these preprocessing steps which depend on specific applications/preferences and exceed the scope of this review. Specific techniques used in this publication are elaborated in chapter 3 of this work.

Finally, processed spectra may then be used for machine learning based approaches. Classifiers are trained on datasets with Raman spectra of known origin and used on unlabeled spectra to assess their performance. Multivariate differences in peak expressions/intensities across different classes of spectra lead to successful classification. A wide variety of techniques may be employed[20][21] which exceed the scope of this literature review though optimal classification is generally achieved by using automated approaches to detecting key features for separation of classes such as support vector machines (SVMs). The following chapter of this review will focus on specific examples while the techniques employed for this project are detailed in chapter 3.

2.3 Diagnostic applications of Raman Spectroscopy in Oncology

RS has been studied for a variety of clinical applications such as in the diagnosis of Alzheimer's disease[22], nephropathic cystinosis [23], studying calcification in cardiovascular applications[24], [25],[25]. The focus of this review will be on oncological applications where currently available diagnostic tools for tissue characterization fail to address the needs of clinicians. These include H&E/histopathology on biopsy samples, computed tomography, magnetic resonance imaging and positron emission tomography scans and ultrasound. H&E/histopathology is lengthy, labor intensive, costly and can only provide results days following the surgery[26]. The other imaging techniques lack in sensitivity and specificity for cancer cell detection, can be very expensive, oftentimes rely on the use of an exogenous contrast agent, and can not be used in real time. RS is a label-free, minimally invasive and sensitive technique which can be used in real-time and holds great promise for applications in oncology. The following section will review literature in this domain with an emphasis on clinical applications in prostate and *in vivo* applications in humans. In prostate, RS has been shown to identify cancer with high accuracy. A few studies using Raman microscopy-based systems have successfully characterized prostate cancer tissue. Crow et al. first

suggested the use of RS in prostate in 2002 showing variations in expressions of peaks corresponding to glycogen and nucleic acids (1655 cm^{-1} and 1240-1265 cm^{-1}) between spectra collected using a Raman microscope on benign prostatic hyperplasia (BPH) and prostatic adenocarcinoma[27]. A year later, this group conducted a study involving 27 patients showing RS could be used *in vitro* to identify BPH (sensitivity 93%, specificity 92%) , gleason scores (GS) <7 (sensitivity 85%, specificity 96%), =7 (sensitivity 81%, specificity 96%) and >7 (sensitivity 94%, specificity 100%)[28]. This was accomplished using a linear discriminant analysis (LDA) classifier with a leave-one-spectrum-out cross validation approach. Crow et al. again demonstrated the potential of RS *in vitro* using a Raman microscope to differentiate (classification performed using LDA and leave-one-spectrum-out cross validation) between spectra from two well differentiated and two poorly differentiated cell lines with sensitivity and specificity at 96-100% and 99-100%, respectively[29]. Wang et al. have also demonstrated that a Raman microscope on two cell lines from 50 patients can successfully discriminate between androgen-dependant and castration-resistant prostate cancer using an SVM trained with leave-one-out cross validation with a sensitivity of 88.2% and specificity of 87.9%[30]. Similar Raman microscopy studies have been performed on bladder breast, skin, oral, and a host of other cancerous tissues with equally promising results[31],[32]. These studies all suggest promise for the use of RS as a diagnostic tool though the use of RS through a microscope imposes significant limits on its clinical usefulness and viability. Microscopes require tissue preparation/fixation, have long acquisition times (in the order of 10 seconds to one minute per spectrum) and therefore fail to address the need of real time characterization in the operating room. As such, much work has been done to integrate RS to fiber optic probes. Due to the difficulty of acquiring histopathology ground truth *in vivo* most studies have been geared towards analyzing tissue *ex vivo* as a first step towards testing systems and probes compatible for *in vivo* use[33]. A 2005 study on snap-frozen bladder and prostate samples collected during surgery using a "fiberoptic Raman system suitable for *in vivo* use" was able to differentiate benign from malignant samples with an accuracy of 84% on bladder samples and 86% in prostate samples[34]. Previous work performed *ex vivo* thus shows promise for the application of RS to the characterization of prostate tissue.

The past decade has been marked with important strides towards clinical translation of RS *in vivo*. Technological advances in CCD detectors, lasers, and fibered optics have allowed for spectral acquisitions with performance and time scales suitable for *in vivo* use[15]. Zhao et al conducted a large study on 289 patients where they performed measurements on suspect skin lesions with acquisition times under 1 second. Using partial least squares regression and linear discriminant analysis on the spectra, they achieved 91% sensitivity and 75% specificity for differentiating skin cancers from benign legions and 97% sensitivity/78% specificity in differentiating malignant melanoma from benign pigmented lesions[35]. For more difficult to reach organs, RS has been integrated to a variety of endoscopic systems for investigative work [33]. Draga et al. used an RS probe to obtain Raman spectra from 'suspicious' and 'nonsuspicious' bladder locations with acquisition times under 5 seconds. They reported a sensitivity of 85% and 79% in distinguishing normal from cancerous bladder locations[36]. In brain cancer, invasive cancer cells frequently remain after surgery, leading to disease recurrence and a negative impact on overall survival[10]. Our research group at Polytechnique Montreal has developed a handheld RS probe for intraoperative collection of Raman spectra[10]. The following figure shows a view of the handheld probe used during open cranium glioblastoma resection.

Figure 2.3 : Handheld RS probe developed by Prof. Leblond's research group at Polytechnique Montreal in use during glioblastoma resection surgery

Using this probe, a study was conducted on 17 patients with gliomas of grade 2-4 with acquisition times on the order of 1 second. For each patient, measurements were collected in the surgical cavity by placing the probe in contact with tissue of unknown origin. The surgeon then took a biopsy where the probe left an indentation which underwent histopathological analysis and was classified as being “normal”, “infiltrated” or “cancer”. This allowed the generation of a dataset with 161 spectral measurements with a histopathological oncological assessment as ground truth. Typical spectra for each class as well as a corresponding histopathology slide are presented in the following figure.

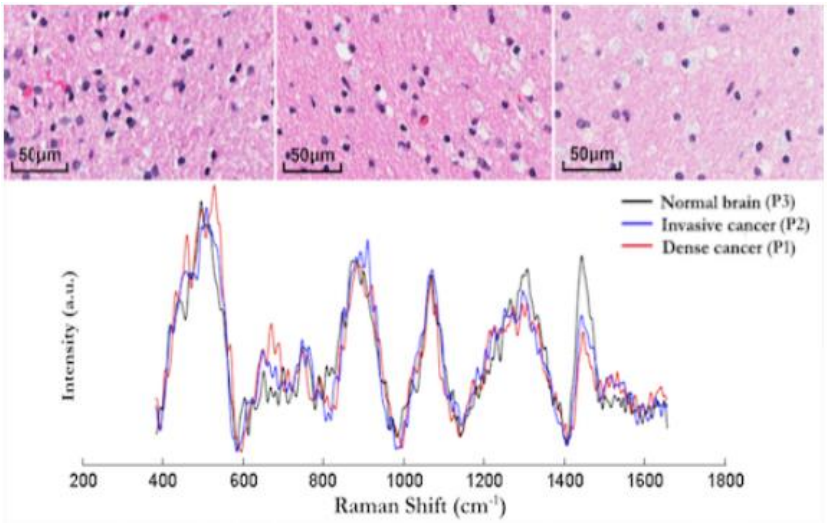

Figure 2.4 (Top) Histopathology images of 3 brain tissue biopsy samples (left: dense cancer tissue, middle: invasive cancer, right: normal tissue) corresponding to locations where RS measurements were made. (Bottom) Raman spectra of the measurement locations showing spectral differences. (Figure reproduced from Jermyn et al. 2015)

Machine learning algorithms (gradient boosted trees) were used with k-fold (10 folds) cross validation on the dataset and yielded a diagnostic accuracy of 92%, with 93% sensitivity and 91% specificity. Using a handheld probe with the same design, Aubertin et al. performed *ex vivo* research on human prostate. They reported detection of prostate cancer in freshly harvested, unprocessed *ex vivo* slices of human prostate following radical prostatectomy. Raman spectra were collected all over the surface of the prostate slices immediately following surgery and each point where data was collected was marked with ink. The prostate slices were then sent for

histopathological assessment and each spectrum was matched to a pathologist's diagnosis. A dataset of 925 spectra (149 cancerous, 776 benign) was obtained from 32 prostates and RS was able to distinguish prostatic from extra prostatic tissue and benign from malignant tissue with sensitivities of 82%, 83%, 86% and 87% respectively[37]. Figure 2.6 summarizes the process of histopathology registration and shows mean spectra collected for benign and cancerous classes.

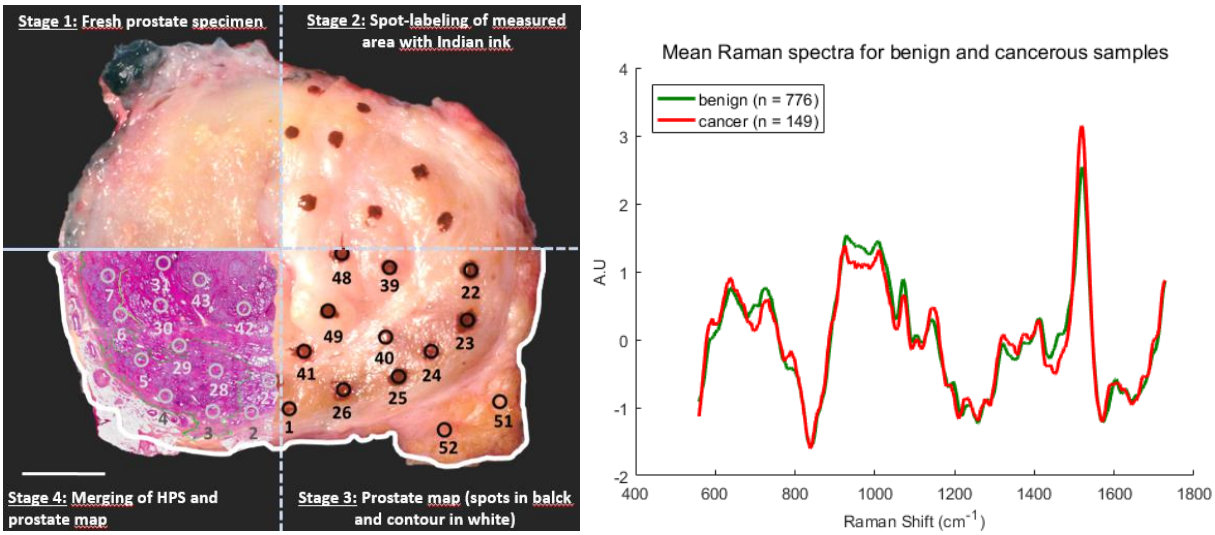

Figure 2.5 (left) Methodology for spatial correlation of Raman spectroscopy measurements and tissue for diagnosis. Prostate specimen is divided into four quadrants to demonstrate each stage of the methodology performed on the same prostate slice (figure on from Aubertin et al. In preparation). (right) Average spectra of 149 spectra from cancerous tissue in red and 776 spectra from normal tissue in green (original figure)

Previous work thus shows successful *in vitro* and *ex vivo* prostate tissue characterization which show promise to address unmet clinical needs in RA-RP. RS probes have also successfully been used *in vivo* on multiple organs with promising results. To our knowledge, this technique has not been applied *in vivo* on prostate yet.

CHAPTER 3 METHODS & RESULTS COMPLEMENTARY TO THE RESEARCH ARTICLE

The following chapter describes the scientific approach employed to achieve the objectives set out in this work. A general overview of the methods employed for the realization of the objectives set out in section 1.3 is presented.

3.1 Objective 1 : Integration of RS to the da Vinci surgical robotics platform

The first objective set out in thesis was the design and development of an RS system, using two excitation wavelengths, adapted for integration to a surgical robotics platform. The system is based on previous systems used by our research team with important modifications outlined in the sections below. First, a general overview of the system is presented followed by each of its components, the work done in assembling them, and the primary hurdles overcome.

3.1.1 Raman spectroscopy system

An RS system adapted for robotic integration was designed and assembled. The system is primarily composed of a spectrometer coupled to a highly sensitive CCD camera, a laser excitation source capable of delivering light at two excitation wavelengths and a fiber optic probe responsible for light delivery and collection. A custom acquisition software coordinates all spectral acquisitions, communicates with system components to set parameters and handles data exchange/storage. The following figure shows the assembled RS system as well as a schematic representation of the connections between its components :

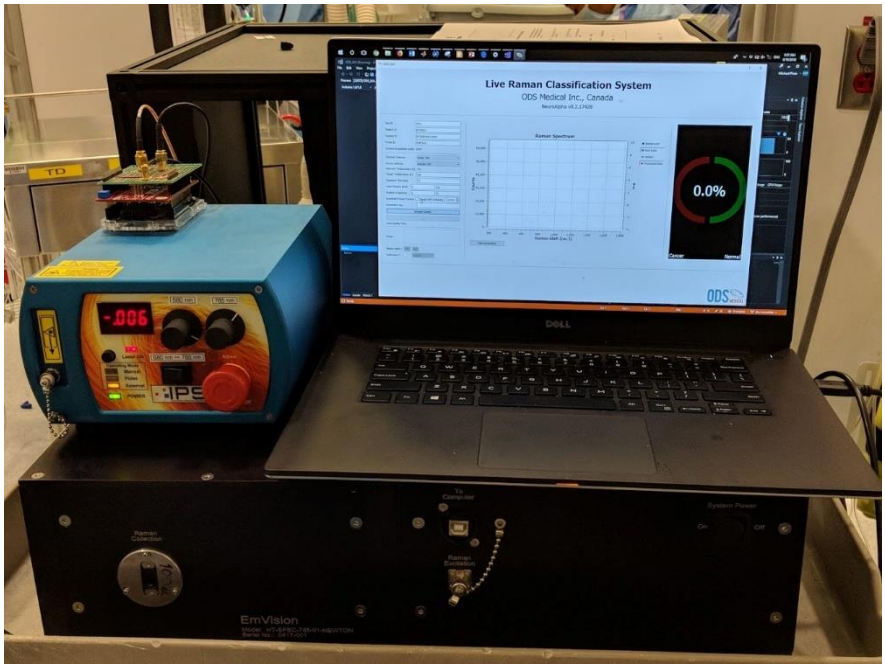

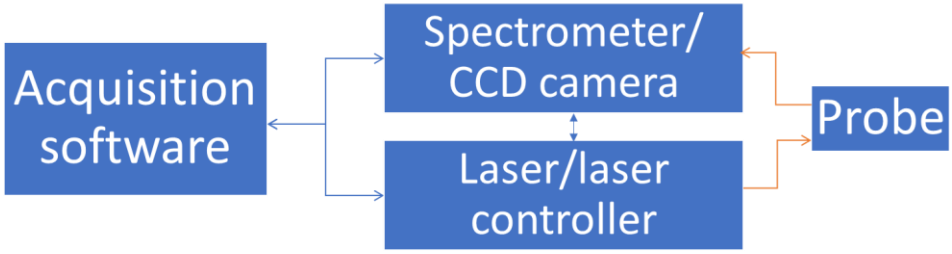

Figure 3.1 : (top) Picture of the assembled RS system with laser, computer running acquisition software and spectrometer. (bottom) Schematic overview of the Raman spectroscopy system components and the connections between them. Blue arrows represent digital/electrical connections while orange ones represent optical/fibered connections.

3.1.1.1 Spectrometer & Camera

A custom spectrometer built by EMVision LLC was ordered for this project.. The spectrometer is optimised for collection in the 800-900 nm range where it has a resolution of ~0.15 nm. This corresponds to the FP region (500-2000 cm^{-1}) of a 785 nm excitation and the HWN region (2500-4000 cm^{-1}) of a 680 nm excitation. Light travels from the RS probe's collection optics through a

150 um slit where it is then diffracted onto the CCD array of a highly sensitive detector (Andor Newton 920 XT). The camera parameters used for all spectral acquisitions in this project were set based on recommendations from colleagues and the industrial partner ODS Medical and are listed in the table below :

Table 3.1 : Acquisition parameters used for the Andor Newton camera

Parameter	**Value**
Detector temperature	-80
Exposure time	75-100 mS
Vertical shift speed	1.8 us
Horizontal shift speed	2.5 MHz
Gain	2x
Image mode	Full vertical binning
Acquisition mode	Kinetic series
Baseline clamp	‘on’

The spectrometer was manufactured by Emvision LLC and built to spec for this project. It is worth noting that initial tests with the spectrometer showed signs of stray light on spectra. This was solved by inserting dark absorbing material on the inner walls of the spectrometer to block unwanted reflections in the system.

3.1.1.2 Raman probe adapted for robotic use

Current Raman probes for *in vivo* use have been designed for handheld use and are too large for robotic integration. As such, a Raman probe was designed for this purpose. From an optics standpoint, the probe has a similar design to the one currently used by industrial partner ODS

Medical for its ongoing clinical trial in humans. The probe consists of a central excitation optical fiber surrounded by 12 collection optical fibers. A bandpass filter on the excitation lens narrows the excitation spectrum while a notch shaped longpass covering only the collection fibers lets through wavelengths in the range of the Raman spectra being measured while filtering out contributions from dominant Rayleigh scattering. The distal lens at the tip of the probe sends the central excitation straight through while focusing captured light back into the collection fibers. From a mechanical standpoint, the outside of the probe casing was designed to be grasped by robotic instruments. It is a 2.5 mm wide and 6.5 mm long cylinder with its side walls flattened in a hexagonal pattern. The parallel flat faces are picked up by standard robotic graspers manufactured by Intuitive (be it a standard needle driver robotic arm or a Prograsp instrument). The following figure shows a close up view of the probe, a blown up view with all its components and a to scale comparison of the current design with the handheld probe used by ODS Medical and in previous studies.

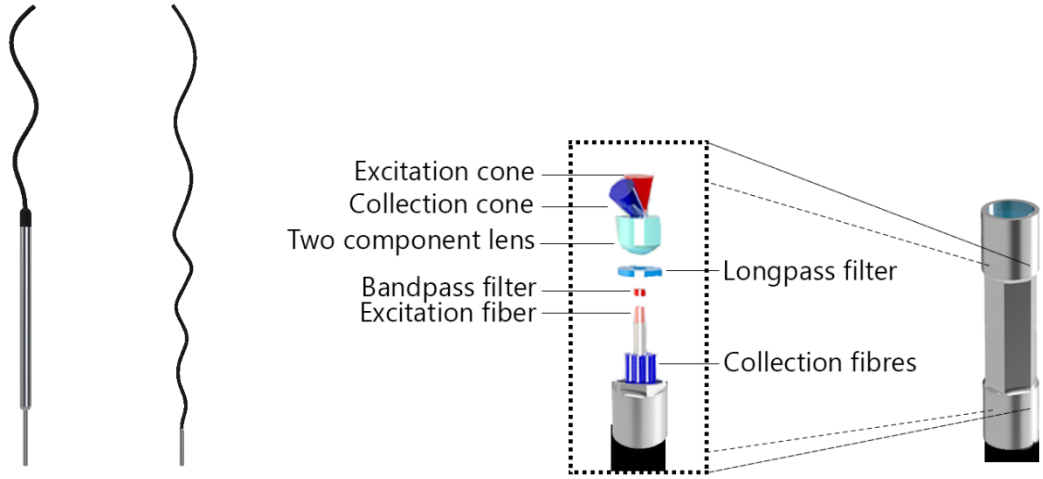

Figure 3.2 : (left) Side-by-side and to scale comparison of the probe designed for robotic integration and the handheld one currently used for surgical interventions by our group and the industrial partner ODS Medical. (right) close-up view of the hexagonal profile machined on the probe tip to facilitate grasping using standard robotic equipment and a blown-up view of the main optical elements of the probe

The distal end of the probe extends into 1.5 m of optical fibres which connect the excitation fiber to the excitation source with an FC/PC connector and the 12 collection fibers to the spectrometer through an MTP connector. The probe and its coating are sterilisable through standard STERRAD procedures.

3.1.1.3 Laser & laser controller

The laser used for Raman acquisitions is equipped with both a 680 nm and a 785 nm diode coupled to a single FC/PC connector. Synchronising laser excitation and spectral acquisition required the development of a board capable of communicating with the laser (to control power and wavelength selection), the spectral acquisition software (to determine which power and wavelength to deploy) and the camera (to ensure synchronisation). The controller was developed using an Arduino Uno, an Analog Shield (Agilent electronics) and a custom shield to make all necessary electrical connections. It consists essentially of a high precision 10 bit DAC which is used to control laser power and a TTL switch which toggles between wavelengths. Laser activation is controlled by monitoring the “FIRE” pin on the Andor Newton camera. The master software sets the wavelength on the laser controller, which then monitors the fire pin for a rising edge. The laser is turned on immediately (within 1 ms of a rising edge) after camera fire and is turned off immediately on a descending edge (within 1 ms of a descending edge) of the camera fire. For safety, a watchdog timer is implemented on the controller to turn off the laser automatically after 500 ms in the event that the fire pin sequence does not function properly.

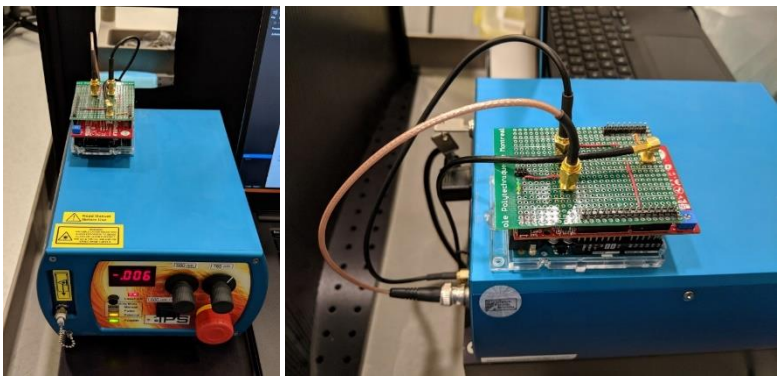

Figure 3.3 (left) Laser & laser controller (right) side view of laser controller with rear connections to laser unit.

3.1.1.4 Software GUI for data acquisition

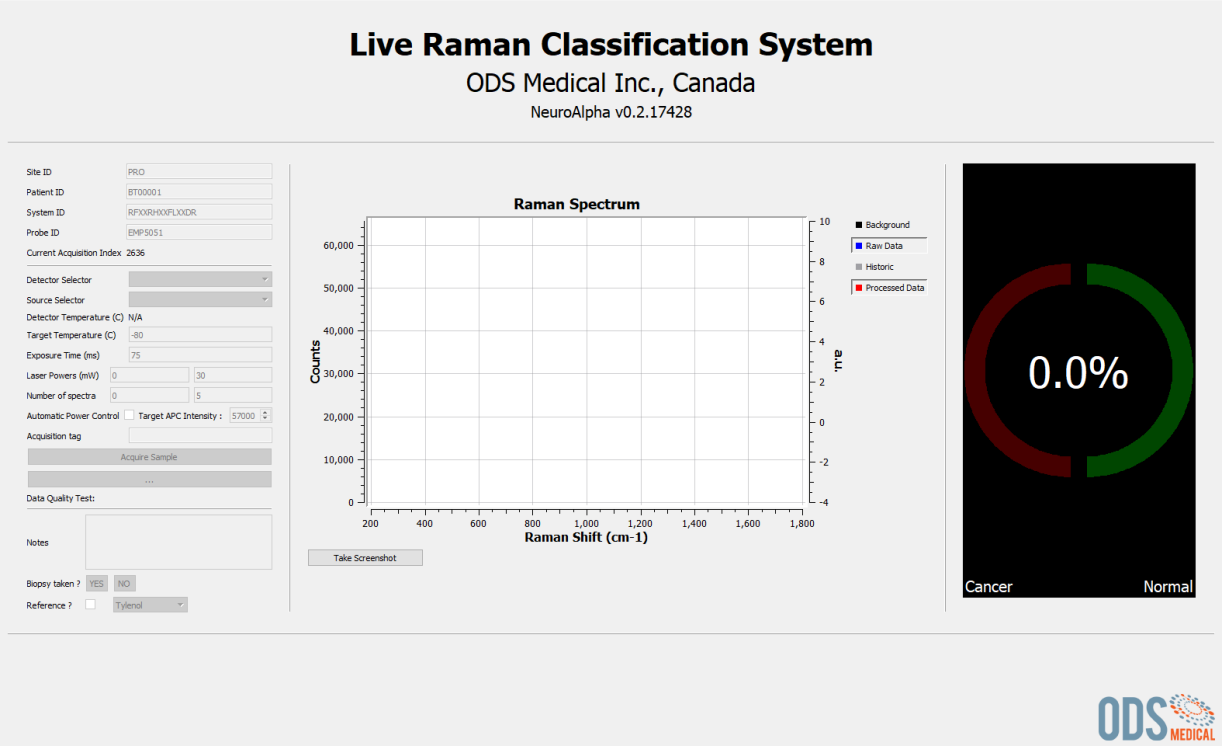

Figure 3.4 : Screenshot of the acquisition software used to perform all spectral measurements

A software GUI is necessary to orchestrate spectral acquisitions, communicate between different system components and store information related to each measurement. The software used for this project is a modified version of ODS Medical's software currently used to acquire Raman spectra with one wavelength. The software (written in C++ using Qt) was heavily adapted for this project. First and foremost, the software was modified to accommodate two excitation wavelengths and interface with a new laser controller. Software was written to calibrate power for both wavelengths, set excitation power, exposure time, and number of spectra independently. Acquisition parameters are communicated to an Arduino based laser controller (section 3.1.1.3) which then interfaces with the laser and camera to perform acquisitions. An automatic power control (APC) algorithm was developed to automatically determines optimal laser power for each laser to occupy the most dynamical range of the CCD detector. When enabled, the APC algorithm performs two single acquisitions per wavelength on the sample prior to performing the full one. Since the relationship

between signal intensity and laser power used is linear, the software uses the dynamical range occupied at each of these two powers to do a linear interpolation of optimal power for each wavelength. In addition to incorporating two wavelengths, the software was modified to allow external platforms to easily perform spectral acquisitions. A TCP/IP server was written which allows clients to simply connect to a specified IP and port to communicate. Optional parameters allow to set specific parameters and send information to identify/landmark acquisitions. The following figure illustrates the simplicity of connecting to the platform with two code snippets (one in matlab, one in python) showing all code required to initiate an acquisition.

```matlab
function response = ODSCommunicate(ip, port,i)

t = tcpip(ip, port, 'Timeout', 3);
fopen(t);
fwrite(t,'go');
fwrite(t,num2str(i));

start = clock;
Timeout = 2;

response = fread(t,1);
while (isempty(response) || response ~=100 )
   response = fread(t,1);

end
response = char(response);

end
```

```python
import socket

# Server adress and communication parameters
TCP_IP = '169.254.113.23'
#TCP_IP = '127.0.0.1'
TCP_PORT = 50382
BUFFER_SIZE = 1024

# Info to send to server
MESSAGE = "go"
ID = "123" # a string used to describe the measure (the ID will be saved to
file with each acquisition)

# conncetion to the server and data exchange
s = socket.socket(socket.AF_INET, socket.SOCK_STREAM)
s.connect((TCP_IP, TCP_PORT))
s.send(MESSAGE)
s.send(ID)

#the server will return a 'RCCC' string after a succesful acquisition where :
# R is the classifer result (0 - no classification, 1 - class 1 , 2 - class 2
(classifier dependant) )
# CCC is a number between 0 and 100 representing classifier confidence
data = s.recv(BUFFER_SIZE)
print(data)
```

Figure 3.5 : examples of TCP/IP protocol required to communicate with the RS platform via a specified IP/Port in Matlab (left) and Python (right)

3.1.1.5 Raman shift (x axis) and relative intensity (y axis) calibration

X-axis and relative intensity correction are performed using molecular standards (acetaminophen & NIST 2241 respectively). X-axis to pixel correspondence is obtained using a 785 nm fingerprint Raman spectrum of Tylenol. Peaks from the spectrum obtained by the system are compared to reference peak positions (using a purpose built GUI shown in the following figure) and a polynomial fit is used to compute the x-axis to pixel correspondence of the measured spectrum.

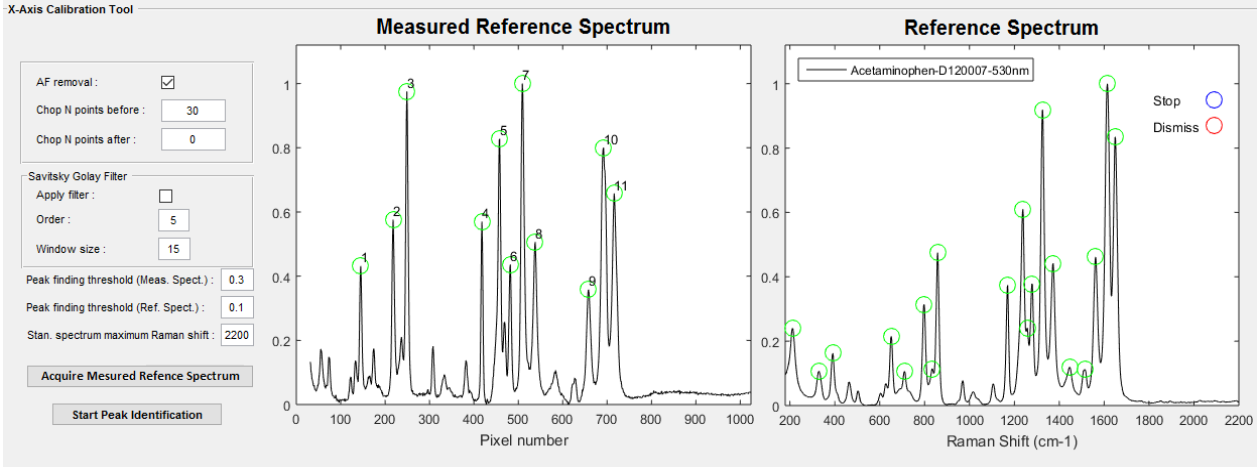

Figure 3.6 : software used to compute x-axis to pixel correspondence of the spectrometer. Peaks from a measured Tylenol spectrum are matched to their corresponding peaks on a reference spectrum one by one.

The following figure shows the measured spectrum plotted against it's calibrated x-axis with an overlay of the reference spectrum showing proper peak alignment.

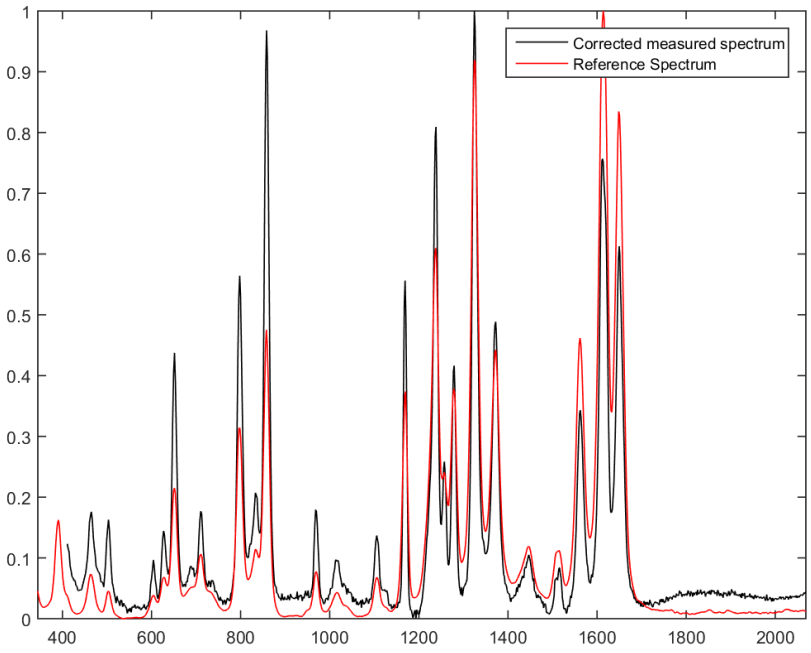

Figure 3.7 : calibrated measured spectrum overlayed with reference spectrum showing proper peak alignment

This technique is not suitable for the high-wavenumber (680 nm excitation) spectrum because of a relatively low peak count. As such, x-axis calibration for high-wavenumber spectra is calculated using the precise excitation wavelengths (within 0.15 nm) provided by the laser manufacturer. The calibrated x-axis is converted from wavenumbers to corresponding nm and back using precisely known excitation wavelengths and the following equation.

$$\Delta w = \left(\frac{1}{\lambda_0} - \frac{1}{\lambda_1}\right) \left| \begin{array}{c} \lambda_0 is\ the\ excitation\ wavelength\ (nm) \\ \lambda_1 is\ the\ spectrum\ wavelength\ (nm \\ \Delta w\ is\ the\ Raman\ shift\ (cm^{-1}) \end{array} \right.$$

Relative intensity (y-axis) correction is obtained using a NIST 2241 relative intensity correction fluorescence standard. The standard is provided with a certified polynomial for the theoretical spectrum($I_{SRM}(\Delta w)$) of the standard which relates the relative spectral intensity to the Raman shift. Dividing the theoretical curve by a measured spectrum of the standard ($S_{SRM}(\Delta w)$) can be used to determine a spectral intensity-response correction ($I_{corr}(\Delta w)$) unique to the Raman system[19]. This correction curve can then be used to obtain Raman spectra ($S_{corr}(\Delta w)$) that are corrected for a number of, but not all, instrument-dependent artifacts[19] through simple element to element multiplication. The following equations summarize the process of relative intensity correction applied to each processed spectrum.

$$I_{SRM}(\Delta w) = A_0 + A_1 * (\Delta w)^1 + \cdots + A_5 * (\Delta w)^5 \left| \begin{array}{c} A_n\ are\ certified\ polynomial\ coefficients \\ \\ \Delta w\ is\ \ Raman\ shift\ (cm^{-1}) \end{array} \right.$$

$$I_{corr}(\Delta w) = \frac{I_{SRM}(\Delta w)}{S_{SRM}(\Delta w)}$$

$$S_{corr}(\Delta w) = \ S_{corr}(\Delta w) * I_{corr}(\Delta w)$$

3.1.2 Clinical integration & workflow

The modified probe is designed to be inserted to the patient using a “drop in” approach. The Raman probe is inserted to the patient through a laparoscopic port. This can either be the port used for the camera endoscope or a laparoscopic assistant port. Assistant ports are insertions commonly used in RA-RP surgery which are placed 5-10 cm away from robotic arm ports for surgical assistants to insert classic laparoscopic instruments during the surgery. Trocards span these ports and commonly have diameters between 8-12 mm leaving 5.5 – 10.5 mm of clearance for the probe fiber to move when being manipulated. When the surgeon is ready to use the RS probe, the laparoscopic assistant removes it from its sterile packaging and feeds it through the chosen port. Once the probe is inserted to the patient, the surgeon uses may use his instruments to grasp it and prepare for RS measurements. The following figure shows a CAD rendered view of the proposed approach.

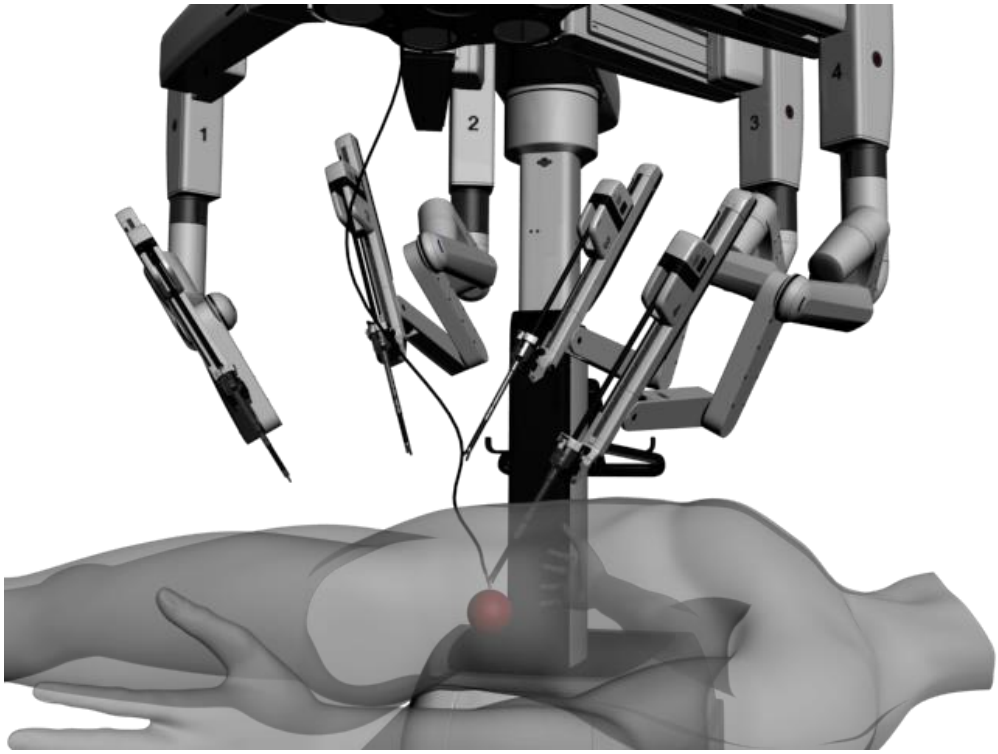

Figure 3.8 : 3D rendered representation of integration to the patient. The probe is inserted through an accessory or camera port and manipulated by a standard da Vinci laparoscopic instrument to reach the target anatomy (red)

Once the probe is inserted to the patient and picked up by a da Vinci arm, the surgeon and clinical staff coordinate with the RS system operator to perform acquisitions as follows :

1. The surgeon/operator places the probe on the area to be interrogated.
2. The surgeon gives an audible cue to perform the acquisition.
3. The Raman operator performs an acquisition and gives an audible cue when it is done.
4. The surgeon/operator communicates landmarking information to the RS system operator who logs it in the software with the corresponding measurement.

3.1.3 System validation

System validation was performed using a custom made 3d-printed phantom filled with identical silicone insertions. The RS system coupled to a da Vinci robot manipulated by a trained surgeon was used to perform spectral acquisitions on each of the insertions putting the probe at various angles and spectra were compared for repeatability. More details and results on this process are presented in section 4 of this thesis.

Complementary to the phantom evaluation, light contributions from the da Vinci robot's LED based endoscopic illuminator were measured using the spectrometer to assess whether they would have an impact on spectral measurements taken *in vivo*. The following figure shows background spectra (laser powered off) acquired with both the illuminator 'on' and 'off'.

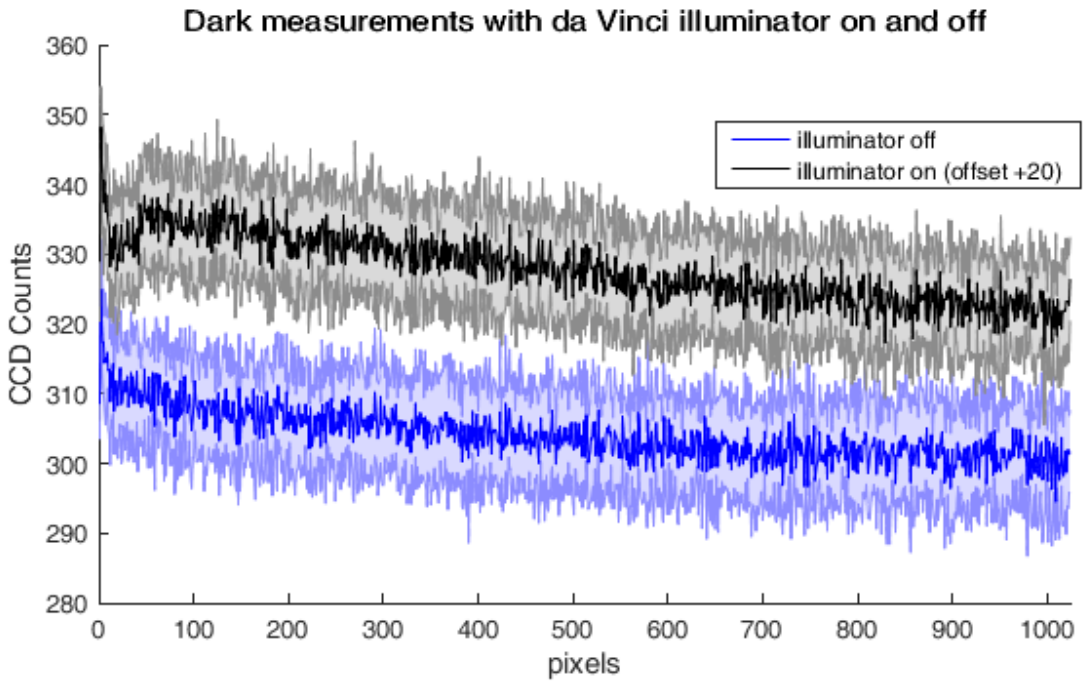

Figure 3.9 : light contribution of the da vinci illuminator on a background measurement when 'on' and 'of'

Both ‘on’ and ‘off’ background spectra show no sharp peaks and very weak intensities when compared to the signal of interest : they occupy roughly 300/62000 CCD counts while the raw Raman/fluorescence signal occupies ~20-60000/60000 CCD counts. Based on these findings the illuminator was kept ‘on’ during *in vivo* measurements described in section 3.2.2.

3.2 Objective 2: Collect *ex vivo* and *in vivo* Raman spectra from human prostate and peri prostatic organs/tissues

Gathering a large dataset is an essential requirement to assessing the potential of RS to perform prostate tissue characterization. Due to the difficulties associated with gathering *in vivo* spectra, a larger *ex vivo* dataset was first acquired to assess classification potential. *In vivo* data was then acquired on 5 patients as a first step towards gathering a comparable dataset and a proof of concept of the feasibility of performing RS *in vivo* during RARP.

All components of this study were approved by the institutional ethics Review Board (CHUM Research Center, Montreal, Canada, REB #17.149), and all methods were performed in accordance with the relevant guidelines and regulations.

3.2.1 Collect Raman spectra from whole prostates following RP

RS measurements were performed on the surface of whole, unprocessed, freshly excised human prostates immediately following RP on 20 patients. To perform these measurements, the RS system was placed on a mobile cart which was brought directly to the operating theatre at the end of RA-RP procedures. Measurements were performed in a light-tight box equipped with an articulated arm used to secure the probe during measurements as depicted in the following figure :

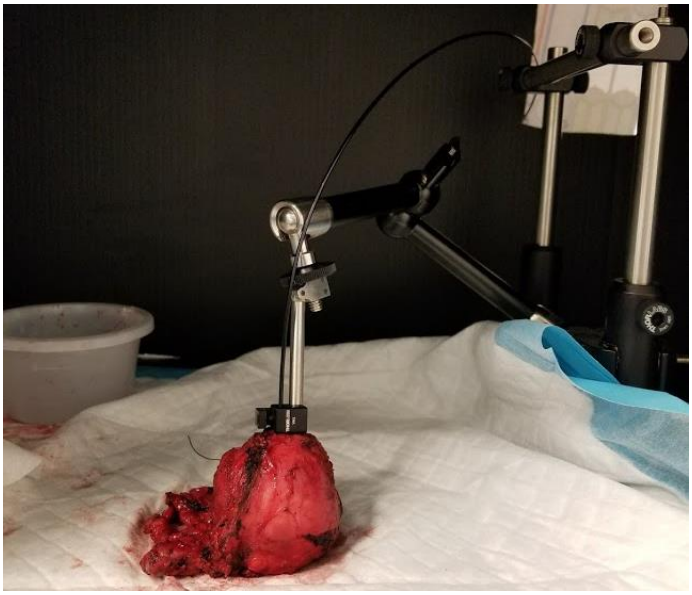

Figure 3.10 : inside the light-tight box used to perform RS acquistions *ex vivo* at the end of RA-RP

For measurements, the prostate was visually segmented into gross anatomical regions and ~5 spectra per prostate were acquired at each of the following:

1. The apex region

2. The base region
3. The posterior region
4. The left lateral lobe
5. The right lateral lobes

Spectra were also collected on the following extra-prostatic structures when sufficient tissue was present following RP :

1. The seminal vesicles
2. The vas deferens canals

Each RS acquisition consists of a fingerprint (785 nm excitation) and a high wavenumber (680 nm excitation) taken sequentially with the acquisition parameters listed in table 3.2.

Table 3.2 : Range of acquisition parameters used throughout the *ex vivo* and *in vivo* experiments

Excitation wavelength (nm)	Spectral range (cm^{-1})	Exposure time (mS)	Delivered power (mW)	# of spectra per acquisition	Camera gain
680	500-2000	100	0-150	10-15	2X
785	2500-4000	100	0 -150	10-15	2X

Spectra were acquired collected across patients and anatomical origin will be compared to assess the feasibility of using RS as a tool to characterize prostate tissue and distinguish prostatic from extra prostatic tissue/organs. Details on the amount of spectra collected from each region and number of patients can be found in chapter 4 of this thesis.

3.2.2 *In vivo* data collection during robotic-assisted radical prostatectomy procedures

The system presented above was used during RARP to collect data from 5 human prostates *in vivo*. Data was collected in the same anatomical regions of the prostate as the *ex vivo* portion o the sreseach

Table 3.3 : Distribution of *in vivo* Raman spectra acquired in surgical cavity during radical prostatectomy procedures.

Anatomical region	**Sub-region**	**N samples**
Anterior		**7**
	Apex	1
	Base	6
Extra-prostatic		**13**
	Neurovascular Bundle	5
	Seminal vesicles	3
	Bladder	5
Total		**20**

3.2.3 Process automation for cancer detection (automated platform)

A complementary portion of this work consisted of working on the automation of data acquisition for prostate cancer research developed by Aubertin et al. Aubertin's method (results available in literature review) consists of acquiring Raman spectra on a cross section of prostate harvested immediately following RP. Roughly 50 spectra are acquired on a ~ 1 cm cross section of prostate and each point interrogated is manually labelled with a dot of ink. The prostate slice is then sent for histo-pathological analysis which provides a diagnosis for each of the labelled spots of ink.

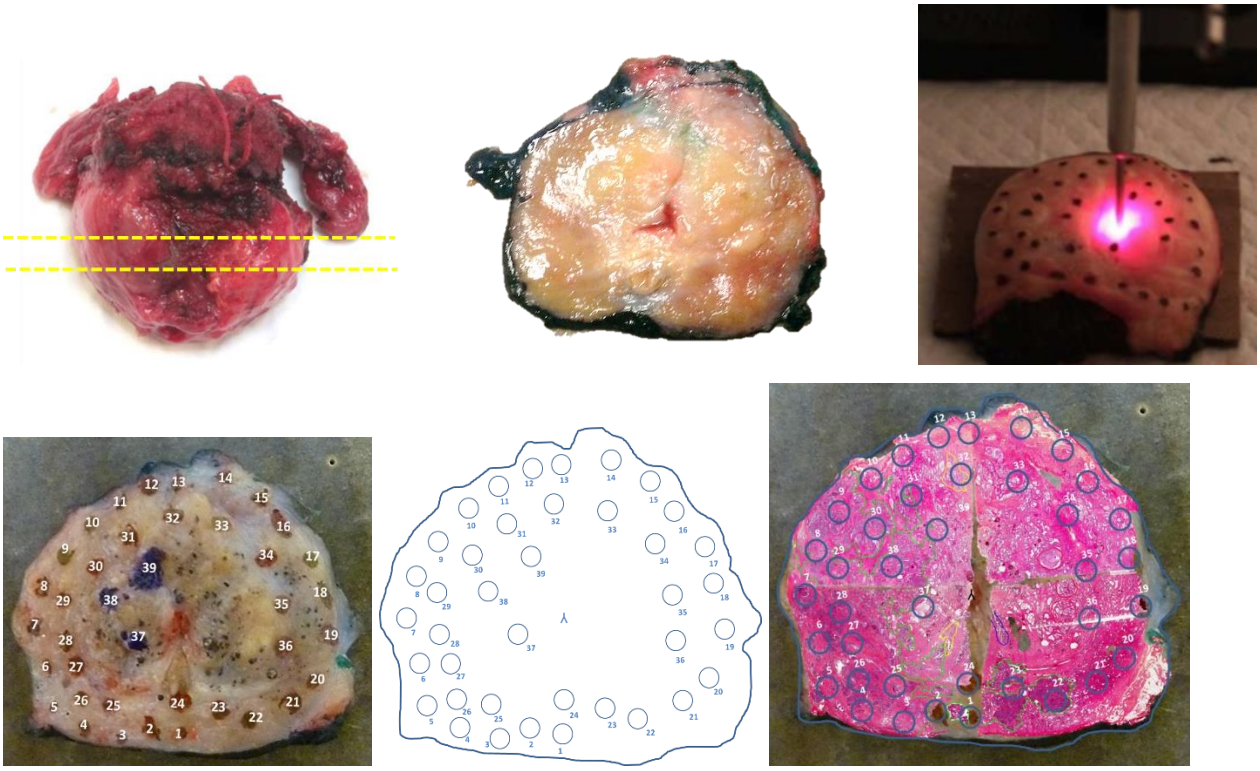

Figure 3.11 : current process for performing Raman measurements on a prostate slice and obtaining registration from histopathology.

Useful machine learning based application of these datasets require large amounts of data. While this process works, it is both lengthy and labor intensive. As such, through supervision of and collaboration with a group of 4th year engineering students at Polytechnique Montreal this process was fully automated.

Automation was achieved by modifying a readily available and open source 3D printer to accommodate a Raman probe. The platform is equipped with a bird's eye view camera which provides an overhead view of the measuring base. A graphical interface (coded in Matlab) allows the user to select points to be interrogated on the specimen graphically. Once all points are selected, the platform begins acquiring spectra by repeating the following sequence :

1. The probe is placed n cm (user configurable) above the platform.
2. The probe is displaced above the point selected in the XY plane.

3. The probe descends ~0.5 mm at a time until contact with the point selected is achieved. Contact is detected by monitoring a modified digital kitchen scale placed below the sample.
4. The platform communicates with the ODS Raman acquisition software and an acquisition is performed. An acquisition ID is sent to the ODS software which is logged with the spectral data.
5. The probe is lifted n cm and once again communicates with the ODS software. A low power acquisition is performed to assess whether the probe tip needs to be cleaned.
6. Steps 1-4 are repeated until all points selected by the user have been interrogated

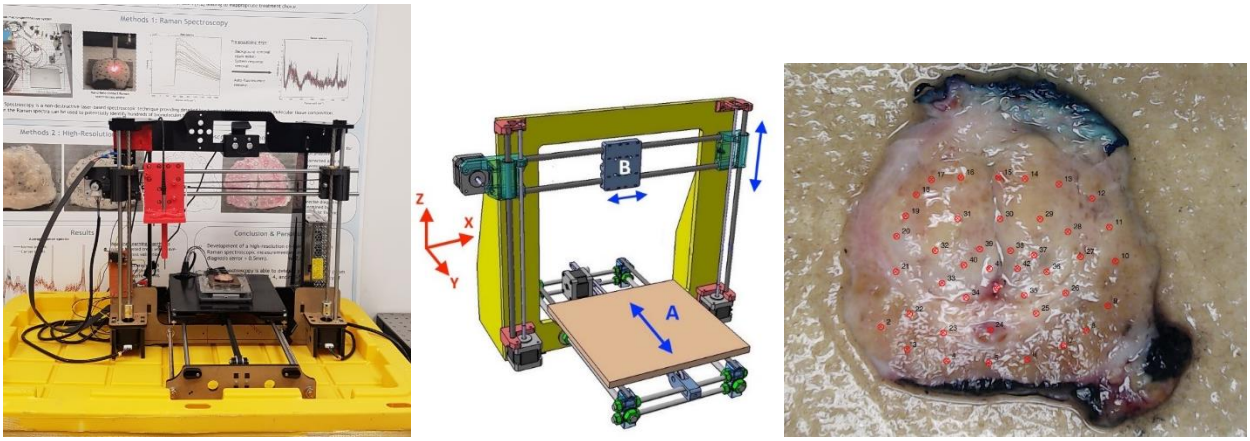

Figure 3.12 : (left) Conceptual view of automated platform. (center) Complete working version of automated Raman platform. (right) mask generated from platform camera image for registration with histopathology

Platform positioning accuracy was validated to be <1 mm by substituting the probe with a marker and selecting points on a sheet of millimetric paper

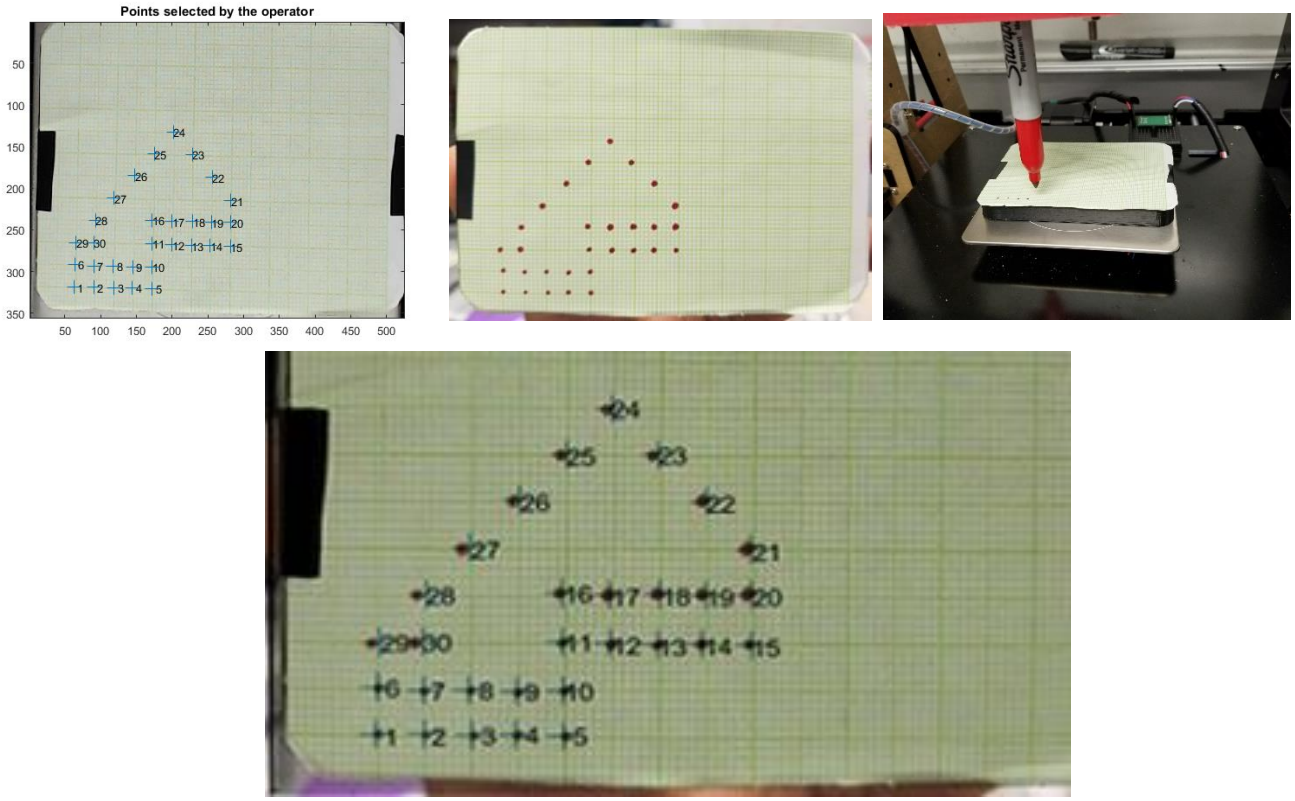

Figure 3.13 : Evaluating platform precision : a marker was mounted on the platform instead of the Raman probe. Points were selected on milimetric paper using the platform software and distance between point selected and point inked was measured

3.3 Objective 3: Classification/tissue characterization based on acquired datasets

3.3.1 Objective 3.1 : Train algorithms capable of differentiating prostatic from peri-prostatic tissue

Spectra originating from the prostate (apex, base, lateral lobes, anterior face) were grouped together and labelled as ‘prostate’ spectra while spectra collected on surrounding anatomy (vas deferens, seminal vesicles) were labelled ‘extra prostatic’ based on clinical utility defined by a urologist and

pathologist collaborating on the project. The Matlab classification toolbox was then used to test a variety of different classifiers and assess their performance on the dataset. Among these were LDAs,, regular SVMs and SVMs with quadratic or cubic kernels. A holdout validation approach was used where 75% of the initial dataset is used as a training set while 25% is set aside to assess performance of the trained classifier. Most classifiers performed reasonably on the dataset though quadratic/cubic SVMs returned the best performance. The following figure illustrates the workflow in assessing classification performance while results are presented in chapter 4 of this thesis.

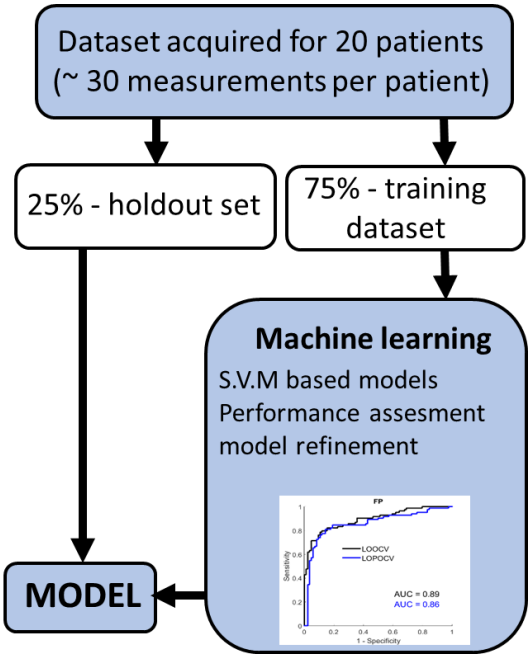

Figure 3.14 : Classification workflow used for characterizing prostate vs extra-prostatic tissue.

CHAPTER 4 ARTICLE 1 : INTEGRATION OF A RAMAN SPECTROSCOPY SYSTEM TO A ROBOTIC-ASSISTED SURGICAL SYSTEM FOR REAL TIME TISSUE CHARACTERIZATION DURING RADICAL PROSTATECTOMY PROCEDURES

The work outlined above set the stage for a peer reviewed publication in the Journal of Biomedical Optics which is currently submitted and awaiting peer review. The following chapter presents this article as it was published. The publication is titled "Integration of a Raman spectroscopy system to a robotic-assisted surgical system for real time tissue characterization during radical prostatectomy procedures' and its authors are the following :

Michael Pinto[a,b], Kevin C. Zorn[b], Jean-Philippe Tremblay[a], Joannie Desroches[a,b], Kelly Aubertin[a,b], Eric Marple[d], Chris Kent[c], Frederic Leblond*[a,b], Dominique Trudel*[b], Frederic Lesage*[a,e]

aPolytechnique Montreal, CP 6079, Montreal, Canada, H3C3A7

bCentre de Recherche du Centre Hospitalier de l'Université de Montréal, 900 rue Saint-Denis, Montreal, Canada, H2X0A9

cODS Medical, 5155 Avenue Decelles, Montreal, Canada, H3T2B2

dEmVision LLC, 1471 F Road, Loxahatchee, U.S.A, 33470

eCentre de Recherche de l'Institut de Cardiologie de Montréal, 5000 Bélanger Est, Montréal, Canada, H1T 1C8

*these authors contributed equally to this work

4.1 Abstract

Surgical excision of the whole prostate through a radical prostatectomy (RP) procedure is part of the standard of care for prostate cancer. Positive surgical margins (cancer cells having spread into surrounding non-resected tissue) occur in as many as 1 in 5 cases and strongly correlate with disease recurrence and the requirement of adjuvant treatment. Margin assessment is currently only performed by pathologists hours to days following surgery and the integration of a real-time surgical readout would benefit current prostatectomy procedures. Raman spectroscopy (RS) is a promising technology to assess surgical margins: its *in vivo* use during RP could help insure the extent of resected prostate and cancerous tissue is maximized. In this work, we thus present the design and development of a dual excitation RS system (680 nm and 785 nm excitations) integrated to the robotic da Vinci surgical platform for *in vivo* use. Following validation in phantoms, spectroscopic data from 20 whole human prostates immediately following RP was obtained using the system. With this dataset, we were able to distinguish prostate from extra prostatic tissue with

an accuracy, sensitivity, and specificity of 91%, 90.5%, and 96% respectively. Finally, the integrated RS system was used to collect preliminary spectroscopic data at the surgical margin *in vivo* in 4 patients.

Keywords: Raman spectroscopy, prostate cancer, robotic surgery.

4.2 Introduction

Prostate cancer is the second most frequently diagnosed cancer world-wide[1]. In the United States, in 2015, there were an estimated 220,800 new cases and 27,540 deaths, namely approximately 9% of all cancer-related deaths[2]. Surgical excision of the whole prostate through radical prostatectomy is an important part of the standard of care for prostate cancer. Recent large surveys of the SEER and National Cancer databases show an increase in the use of radical prostatectomy to 40-55% of cases while rates of radiotherapy based treatment have decreased for medium and high risk patients over the past decade[38], [39]. Radical prostatectomy procedures can be performed either using open or minimally invasive techniques (classic laparoscopy or robotic-assisted surgical methods). Minimally invasive techniques have comparable clinical outcomes, however robotic-assisted prostatectomy procedures lead to shorter hospital stays, less blood loss and reduced complication rates[3]. Furthermore, robotic surgery provides magnified, stereoscopic, high definition visualization, a wide range of motion (7 degrees of freedom), elimination of tremor, and surgeon comfort at a seated console[40]. Adoption of robotic surgery systems has also been rising over the last decade: a retrospective study of more than 500,000 prostatectomies performed in the U.S. found adoption rates for robotic surgery leaping from 0.7% in 2003 to 42% in 2010[41].

The clinical objective of a radical prostatectomy procedure is the complete removal of the organ while sparing nerves and other surrounding tissues. Removing the entirety of the prostate is made difficult by the lack of a clear histologic capsule which often results, in part due to limitations of current tissue imaging techniques, in prostate tissue being left in the surgical cavity after the procedure in as many as 29% of cases[4]. This is an important clinical problem often leading to biochemical recurrences, namely a rise in the blood level of prostate-specific antigen (PSA) in prostate cancer patients after the surgical treatment, which may misleadingly be interpreted as

disease recurrence. However, none of the currently available technologies to identify cancerous tissue (including histopathology, computed tomography (CT), magnetic resonance imaging (MRI), positron emission tomography (PET) scans and ultrasound) can be used reliably during surgery.

Raman spectroscopy is an emerging technology that has shown promising results for highly sensitive and specific molecular tissue characterization[7], [8], [15]. It is based on the detection of inelastically scattered light following tissue excitation with near-infrared light. The resulting spectral shifts are associated with molecular vibrations and provide an avenue for precise and quantitative fingerprinting since different molecular species have their own spectral signature. Raman spectroscopy has previously been shown by our group to detect glioma *in vivo* during surgery by successfully differentiating normal brain from cancer tissue in 17 patients with grade 2-4 gliomas with a sensitivity of 93% and a specificity of 91%[10]. More recently, a multimodal (fluorescence spectroscopy, diffuse reflectance spectroscopy, Raman spectroscopy) optical cancer detection system was used to show that brain, lung, colon, and skin cancers could be detected *in situ* during surgery with an accuracy, sensitivity, and specificity of 97%, 100%, and 93%, respectively[42]. Raman spectroscopy has also very recently been integrated to a commercial biopsy needle for *in vivo* targeted brain cancer tissue biopsies[43]. More specific to prostate cancer, in a study involving 32 fresh and non-processed human prostate specimens obtained immediately following radical prostatectomy, Raman spectroscopy distinguished prostatic from extra prostatic tissue with sensitivity/specificity of 82%/83%, and benign from malignant tissue with sensitivity/specificity of 87%/86%[37]. Other works have also demonstrated the utility of Raman spectroscopy for prostate cancer detection: It has been shown to identify cancer cells with high accuracy *in vitro* in a study where 4 different cell lines varying from benign prostate cells to prostate adenocarcinoma were identified with a sensitivity and a specificity of 96-100% and 99-100%, respectively[29]. Using 38 prostate samples, classification algorithms trained on 197 Raman spectra were shown to distinguish benign prostate, hyperplasia and inflammation from prostate cancer with an accuracy of 86%[34]. In a study involving 27 patients, prostate cancer could be classified into Gleason scores (GS) <7, =7 and >7 with an accuracy of 89%[28].

Previous Raman spectroscopy work shows promise to leverage the molecular specificity of the method to distinguish both benign and cancerous prostatic tissue from surrounding

organs/structures which in turn could improve outcomes of radical prostatectomy. Robotic-assisted surgical systems provide an ideal platform for the integration and clinical translation of Raman spectroscopy. As such, this work demonstrates the design, engineering and successful integration of a Raman spectroscopy system to a surgical robotics platform, its validation on a phantom, as well as preliminary *ex vivo* and *in vivo* spectroscopic data and associated classification results.

4.3 Methods

4.3.1 Raman Spectroscopy System

4.3.1.1 System Overview

The Raman spectroscopy system is composed of a dual-wavelength laser source, a purpose-built spectrometer (Emvision LLC, Loxahatchee, FL, USA), a high-resolution CCD camera (Andor Newton 920) and a custom probe (Emvision LLC) adapted for laparoscopic use. The dual-wavelength laser (Innovative Photonics Solutions, model # 0811A100-B Fat Boy) provides interchangeable 680 nm and 785 nm excitation to the optical probe through a single optical fiber (0.22 NA, FC/PC connector, 105 μm diameter core). The spectrometer was designed to capture both the fingerprint (785 nm excitation) and high wavenumber (680 nm excitation) Raman spectra through the same slit (width: 150 μm) and grating. Table 1 summarizes the physical properties of the spectrometer for each spectral region.

Table 4.1 : Principal technical specification of the Raman spectroscopy system.

Excitation wavelength (nm)	Spectral range (cm^{-1})	Interrogated area diameter (mm)	Delivered power (mW)	Spectral resolution (nm)
680	2500-4000	0.5	0-150	0.1-0.2
785	500-2000	0.5	0 -150	0.1-0.2

The custom-built probe is a re-design of an instrument developed by our group for work on *in vivo* human brain studies[10]. Briefly, lenses and filters disposed at the distal end of the probe allow for collection of the spectroscopic signal from which the Raman contribution can be isolated using optical fibers: a single central fiber for tissue excitation and 12 concentric fibers for detection (Figure 1). A band-pass 785 nm interference filter is placed in front of the excitation fiber for laser line clean-up and a donut-shaped long-pass filter used in front of the collection to reduce the impact of Rayleigh scattered light in the detection path. The filters also eliminate the silica Raman signal created from the optical fibers. Other than the fact both high wavenumber and fingerprint detection can be achieved with the system, the main difference with respect to our neurosurgery instrument is that the outer casing of the new probe was designed to facilitate robotic grasping. It consists of a 12 mm long stainless steel cylinder with a 2.5 mm (2.3 hex flat to hex flat) outer diameter. The central portion of the outer casing is machined to have a hexagonal cross section such that all opposing faces of the outer portion are flat and parallel making easy to be clamped by a standard grasping instrument such as a needle driver or a ProGrasp (Intuitive Surgical #470093) forceps. The probe is connected to the Raman spectroscopy system through a 3 m-long fiber optics cable wrapped in a housing flexible enough to allow for the probe to be inserted into the surgical cavity and manipulated by the robotic-assisted surgical system.

Spectroscopic data acquisition (CCD detection triggered and precisely timed with laser activation) was coordinated using software written in C++ and Qt. From a high level, the software allows the system operator to perform calibration (see section 2.1.2), set acquisition parameters (laser power, imaging time, camera gain, number of repeat measurements), perform acquisitions, and view results (both raw and processed spectra) in real time. The software also allows for automatic calculation of optimal laser power for each wavelength to occupy maximum dynamic range of the camera by performing low power acquisistions with each wavelength and extrapolating optimal power. Laser power calibration is performed using this software and a powermeter (PM1000D, Thorlabs) prior to each use.

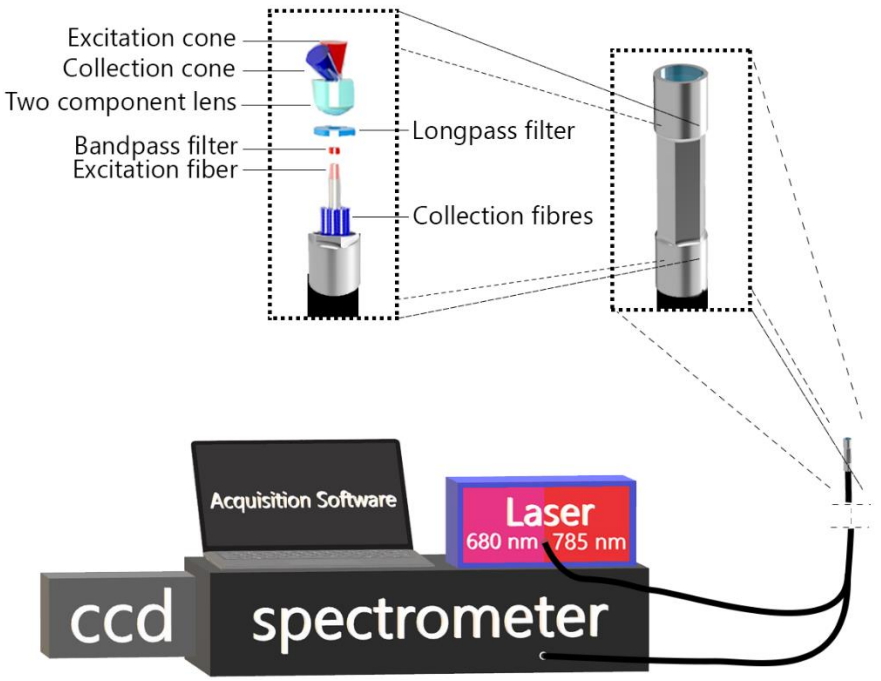

Figure 4.1 : Visual representation of the Raman spectroscopy system designed and built for integration in a robotic-assisted surgical system. Depicted is a close-up view of the hexagonal profile machined on the probe tip to facilitate grasping using standard robotic equipment. A blown up view of the main optical elements making up the probe is shown as well as a schematic representation of the coincident excitation and detection light cones.

4.3.1.2 Spectral pre-processing

Several processing steps were applied to each acquired raw spectrum to isolate the vibrational spectroscopy contribution from background light (*e.g.* ambient light, intrinsic tissue fluorescence) and system response function. Each acquisition consisted in 10-15 consecutive spectra that were averaged together and from which a dark noise measurement (spectrum acquired with laser off) was subtracted to correct for dark noise and ambient light contributions. Spectra were then scaled for relative intensity changes using a NIST 2241 SRM standard[44] lending Raman spectra corrected for the instrument response[19]. Remaining background contributions, including intrinsic tissue fluorescence, were then removed using an automated subtraction algorithm developed by Zhao et al.[13], [17]. The spectra were then smoothed with a Savitsky-Golay filter (of order 3 and with a frame size of 15) and normalized using standard normal variate (SNV) normalization. The calibration of the *x*-axis of the fingerprint spectra was performed by direct comparison with

acetaminophen peaks from the literature[45]. Briefly, peaks on an acetaminophen spectrum measured with the system are manually identified and a second-degree polynomial fit is calculated between measured and literature peaks to generate a calibrated *x*-axis for the system. For the high wavenumber region, the calibrated *x*-axis in wavenumbers for the fingerprint region was converted to nanometers using the known 785 nm excitation wavelength and back to Raman shifts using the known 680 excitation wavelengths (precise excitation wavelengths within 0.1 nm were provided by the laser manufacturer).

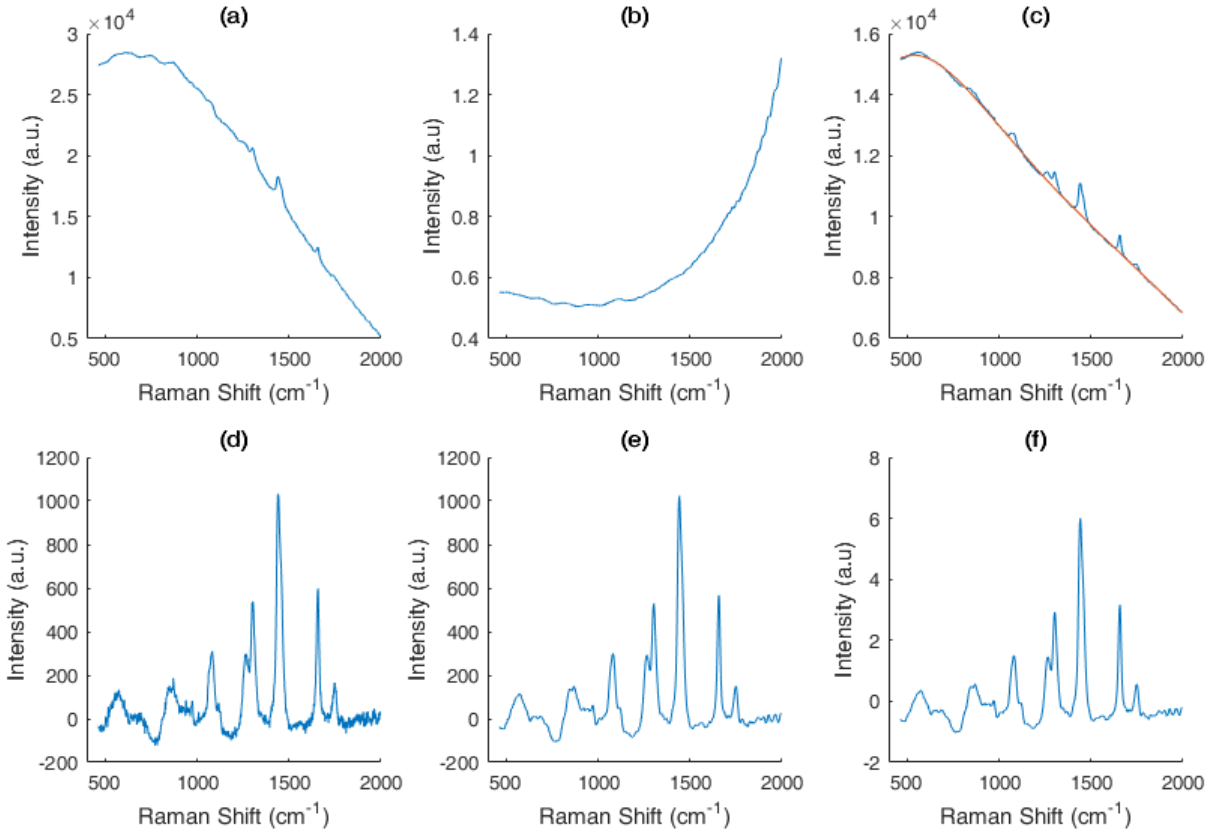

Figure 4.2 : Pre-processing steps for a 785 nm fingerprint *ex vivo* prostate Raman spectrum. (a): Raw spectrum after averaging and dark noise subtraction, (b): NIST correction curve shown for visualisation of instrument response features. (c): raw spectrum multiplied by the NIST correction curve (blue curve) and polynomial fit computed to estimate the fluorescence background contribution (orange). (d): Subtraction of the fluorescence background curve from the NIST corrected raw spectrum in (c). (e): Savitsky-Golay filtered signal to eliminate high frequency noise. (f) : SNV-normalized spectrum.

4.3.1.3 Optical probe integration in a robotic-assisted surgical system

The Raman probe system was integrated with a robotic-assisted surgical system (daVinci Xi, Intuitive Surgical) to allow Raman spectroscopy tissue interrogation during radical prostatectomy procedures. Integration of the spectroscopy system with the robotic-assisted surgical system imposed several constraints on the design, including the fact the probe needed to be inserted into the patient through an assistant port which consists of an 8-12 mm trocar placed through the patient's abdomen. Moreover, the mechanical design needed to allow the surgeon to grasp, manipulate, and immobilize the probe using a standard robotic grasping instrument. Integration also needed to provide enough flexibility to perform measurements at various angles throughout the surgical cavity despite a design based on optical fibers with limited bending radii. Figure 3 provides an overview of the design constraints imposed and how the Raman spectroscopy probe was integrated with the robotic platform to allow intraoperative measurements.

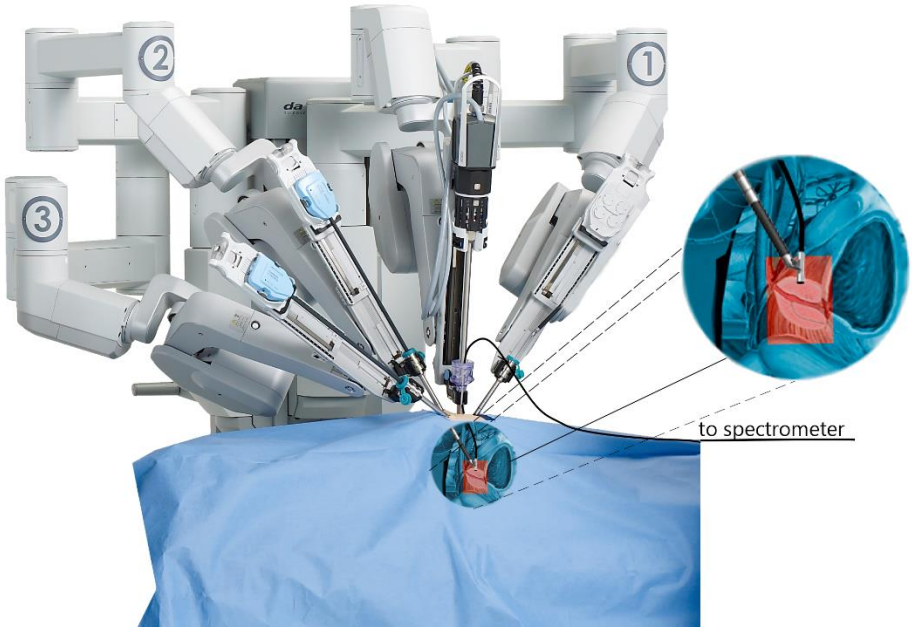

Figure 4.3 : Representation of the Raman spectroscopy probe integrated with the da Vinci robot-assisted surgical system composed of four independently controllable robotic arms (3 visible here, labeled 1, 2 and 3). The arms have interchangeable instruments and the probe was manufactured to be compatible with grasping instruments (such as the Prograsp or needle driving arm

manufactured by Intuitive surgical). The grasping arm is shown ceasing the Raman spectroscopy probe for intraoperative measurements, with a magnified view provided as an aid to visualization.

A phantom was fabricated and used in the scope of an experiment to verify that the integration of the spectroscopy system with the robot-assisted surgery platform allowed repeatable measurements to be achieved over a sufficiently broad range of fiber optics cable curvatures. The phantom consisted of a 6.5 cm-diameter (consistent with the size of a diseased human prostate) hemisphere with regularly spaced 3 mm-diameter insertions along intersecting arcs on the surface (Figure 4a). The insertions were evenly spaced across two perpendicular great circles of the hemispheres (11 for each great circle, ~16° between insertions). The phantom was built using a 3d printer (Prusa i3) and the insertions were filled using a silicone mixture (GE 100% silicone) with clearly distinguishable vibrational spectroscopy features and relatively low fluorescence level. A trained robotic surgeon was asked to manipulate the probe and put it in contact with all insertions along one of the two arcs without letting go of the probe. A spectroscopy measurement was obtained each time contact was made between the probe and an insertion, totalling 11 raw average Raman spectra acquired and processed as described in section 2.1.2. This allowed data to be acquired for various optical cable bending radii for angles (between the main axis of the probe and the base of the phantom) ranging from 0° to 90°.

4.3.2 Data collection on ex vivo human prostates

This portion of the study was designed to characterize Raman spectra associated with prostatic tissue. Spectroscopic data was collected directly on freshly excised whole human prostates following radical prostatectomy. The measurements were performed on a mobile cart equipped with the Raman spectroscopy platform and a light-tight box ensuring minimum levels of ambient light contributions. Using an adjustable arm, the probe was securely placed in contact with freshly excised, non-processed prostate tissue at the plane of resection, the doors to the dark box were closed, and measurements were performed. Specifically, 10-15 spectra per point were acquired, the on-tissue laser power was automatically computed between 0-150 mW using the automated power adjustment routine (see section 2.1.1), camera gain was set to 2X and exposure time at 75-

100 ms per spectrum. Measurements were planned according to grossly estimated prostate anatomy; for each prostate, spectra were collected on the apex, the base, the left and right lateral lobes, the posterior face, the left and, when possible, the right seminal vesicles and the vas deferens canals (Figure 5). The *ex vivo* study was approved by the institutional ethics Review Board (CHUM Research Center, Montreal, Canada, REB #17.149), and all methods were performed in accordance with the relevant guidelines and regulations. More details on the data acquisition protocol can be found in previous work using Raman spectroscopy for prostate tissue characterization[46]. In total 599 spectra were acquired from 20 patients (on average 30 spectra per patient) and grouped by anatomical regions (Table 2).

Table 4.2 : Distribution of *ex vivo* Raman spectra acquired on whole prostates following radical prostatectomy procedures.

	Sub-region	**Number of spectra**
Anterior		383
	Apex	102
	Base	108
	Lateral lobes	173
Posterior		105
Extra-prostatic		111
	Vas deferens	41
	Seminal vesicles	79
Total		599

4.3.3 In vivo data collection during robotic-assisted radical prostatectomy procedures

Raman spectra of prostate tissue near the surgeon's plane of resection around the prostate (at the surgical margin) were acquired *in vivo* using the Raman spectroscopy system in combination with a robotic-assisted surgical platform (daVinci Xi, Intuitive Surgical). The *in vivo* study was approved by the institutional ethics Review Board (CHUM Research Center, Montreal, Canada, REB #17.149), and all procedures were performed in accordance with the relevant guidelines and regulations. Towards the end of the prostatectomy procedure, the probe was inserted into the patient's abdominal cavity and manipulated by the surgeon using a forceps robotic instrument (Intuitive Surgical #470093). The surgeon placed the probe on each point of interest by establishing visual contact between the probe tip and tissue and applying minimal pressure (Figure 7a). Actions were taken to avoid contamination of the Raman spectrum from blood that is not specific to the tissue of interest: 1) the surgeon was asked to avoid areas contaminated by blood, 2) a laparoscopic assistant was present to suction away any excess blood, 3) increased pressure in the abdomen from insufflation (standard for robot-assisted radical prostatectomy procedures[47]) reduced bleeding. Before each measurement, the probe was locked into place long enough to allow spectroscopic data acquisition using the same procedure as described in section 2.2. Measurement locations were chosen by the surgeon to match the gross anatomical regions identified in the *ex vivo* study and were recorded by the Raman system operator. *In vivo* spectroscopic data was acquired during 4 robotic-assisted radical prostatectomy procedures for different prostate regions either associated with prostatic (anterior region only) or extra-prostatic tissue (Table 3).

Table 4.3 : Distribution of *in vivo* Raman spectra acquired in surgical cavity during radical prostatectomy procedures in 4 patients.

Anatomical region	**Sub-region**	**Number of spectra**
Anterior		7
	Apex	1
	Base	6
Extra-prostatic		13
	Neurovascular Bundle	5
	Seminal vesicles	3
	Bladder	5
Total		20

4.4 Results

4.4.1 Integration of the Raman spectroscopy system with the robotic assisted surgical platform

The spectroscopic data acquired for multiple angles on the validation phantom using the Raman spectroscopy robotic-assisted surgical system is shown in Figure 4c. The Raman spectra were computed by evaluating the mean of the spectra measured on the 11 silicone inserts along a hemispheric arc of the phantom. As demonstrated by the small standard deviation (plotted but indistinguishable in the figure), minimal variation occurs across all spectra despite increases in the bending radius of the optics cable. A histogram of the measurements standard deviation was computed to provide a more quantitative representation of the variance (Figure 4d). Measurements were acquired across all points on a 180° arc of the phantom without having to let go of the probe

and without imposing significant bending/strain on the optical fibers. However, the minimum bend radius of the optical fibers is not necessarily a critical consideration with the proposed drop-in design. In fact, the thickest fiber in the probe has a minimum bend radius of ~1.5 mm. Bending this extreme is easily avoidable with this design for two reasons: slack provided by the 1.5 m of fiber allows for larger bend radii and the drop-in design allows for the probe to be picked up at different instrument angles.

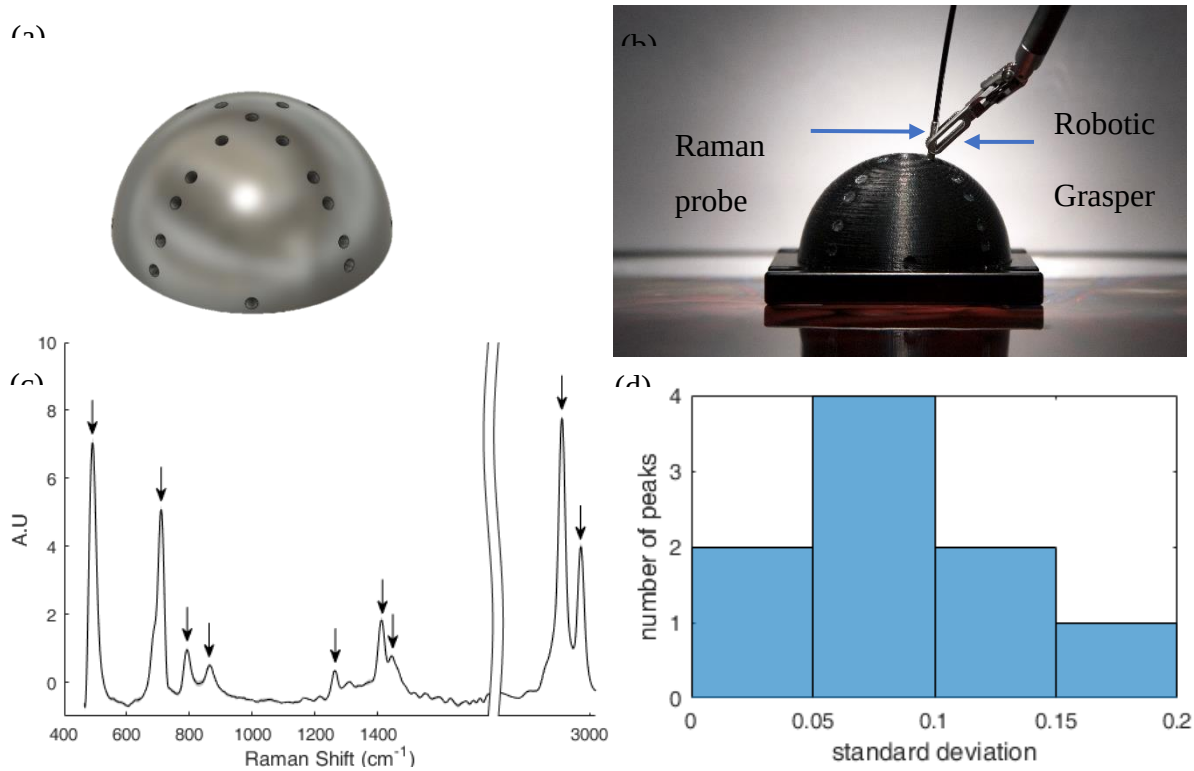

Figure 4 : (a) Conceptual view of the prostate-simulating phantom used for validation, (b) Raman spectroscopy probe manipulated by a surgeon using a robot-assisted surgical system to measure the spectrum of silicone inserts, (c) Mean and standard deviation computed from all SNV-normalized Raman spectra acquired on the silicone inserts with the most prominent Raman peaks of the material identified with arrows. Since the variances in (c) are too small to be visualized, (d) a histogram of the standard deviation between the spectra acquired at each phantom location across all 9 peaks identified is shown in the same units as the processed spectra (*e.g.* 2 peaks have standard deviation between 0 and 0.05)

4.4.2 Ex vivo and in vivo Raman spectroscopy in robotic-assisted radical prostatectomy procedures

Figure 5b shows the mean (across all patients) *ex vivo* Raman spectra for each gross anatomical prostate regions that were interrogated. Several of the main peaks and bands usually associated with biological tissues are identified with numbers (1-14) in the figure, including the phenylalanine peak at 1440 cm^{-1}, the amide III band around 1449 cm^{-1} as well at the amide III band around 1650 cm^{-1}.

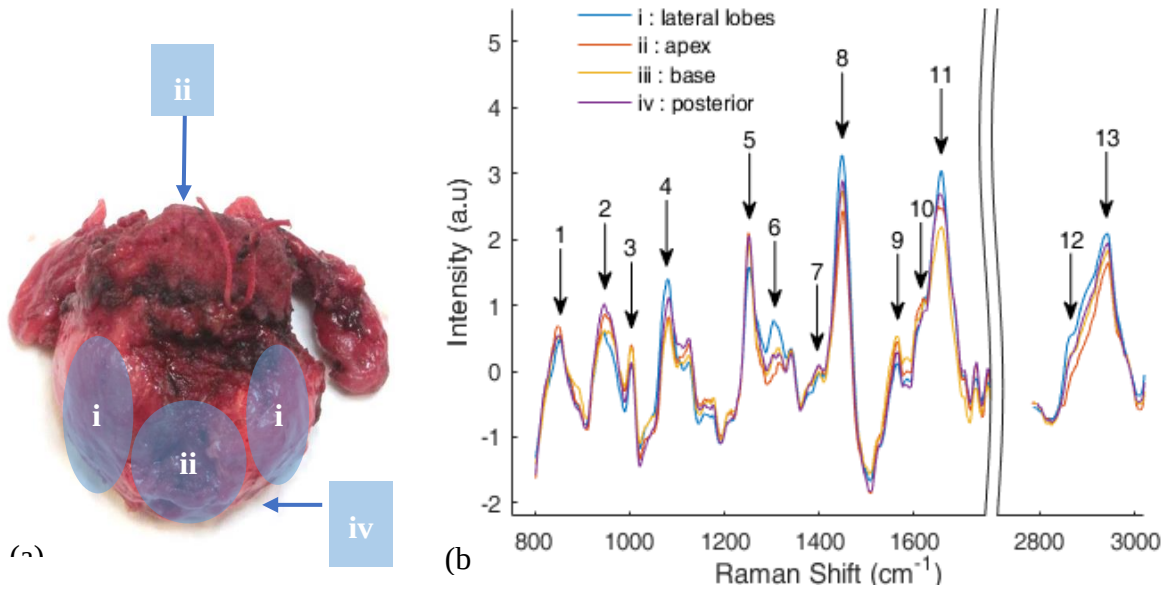

Figure 5: (a) Prostate regions surveyed using the Raman spectroscopy probe: i - left and right lateral lobes. ii - apex. iii - base. iv – posterior. v – seminal vesicles. (b) Mean *ex vivo* spectra measured for each region across 20 patients with prominent Raman bands identified (see Table 4).

Table 4.4 : Prominent biological tissue Raman bands identified on the *ex vivo* prostate spectra.

Band identification label (see Figure 5)	**Wavenumber (cm^{-1})**	**Molecular Bond Assignment**	**Molecular Species**	**Molecules**
1	854	C-O-C	Proteins	Tyrosine
2	950		Proteins	Proline, Valine
3	1004	C-C	Proteins	Phenylalanine
4	1078	C-C/C-O	Phospholipids,,carbohydrates	
5	1252	NH_2	DNA/RNA	Guanine, cytosine
6	1307	CH_2 / CH_3	Proteins, lipids	collagen
7	1398	CH_2 / C=O	Lipids	β-carotene
8	1449	C-H	Proteins, Lipids	
9	1566	CN/NH/COO^- /amide II	Proteins	Tyrosine, Tryptophan
10	1615	C=C	Proteins	Tyrosine, Tryptophan
11	1658	Amide I	Proteins, Lipids, fatty acids	
12	2879	CH_2/CH	Lipids, proteins	
13	2931	CH_2 / CH_3	Proteins	

Spectra originating from the prostate (apex, base, lateral lobes, anterior face) were then grouped together and labelled as ‘prostate’ spectra while spectra collected on surrounding anatomy (vas deferens, seminal vesicles) were labelled ‘extra prostatic’ (Figure 6a). The prominent Raman bands were also observed in the ‘extra prostatic’ tissue measurements, with perhaps the most apparent differences – when compared with prostate tissue – in and around the amide I band. Analysis was then performed to assess the performance of Raman spectroscopy in distinguishing prostate and extra prostatic spectra by creating a classification model using support vector machines. The model was created using the data associated with the full spectrum (no features selection) and was tested on an independent dataset. The later consisted of 25% of all spectra randomly selected across the full dataset ensuring no data from the same patient was used in the training phase. Using this model, prostate tissue could be distinguished from extra prostatic tissue with an accuracy, sensitivity, and specificity of 91%, 90.5% and 96%, respectively. These values were computed from the receiver-operating-characteristic (ROC) curve shown in Figure 6b that has and area-under-the-curve (AUC) of 0.96.

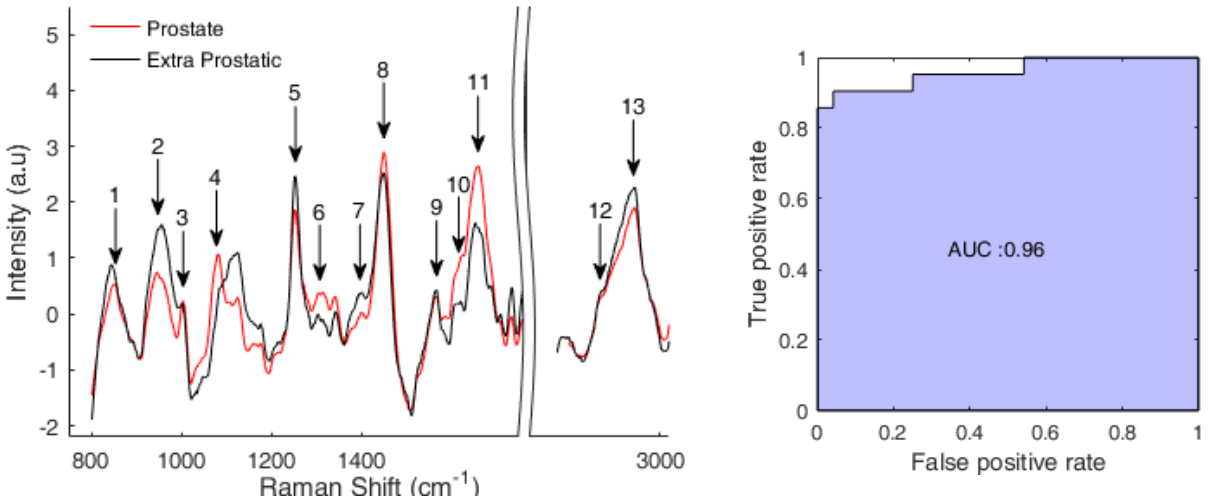

Figure 6 : (a) Mean *ex vivo* Raman spectra for prostate and extra prostatic measurements. (b) ROC curve of corresponding classification result obtained using support vector machines.

Figure 7b shows the average *in vivo* Raman spectra associated with all interrogated prostate areas, showing that same spectral bands and peaks that were identified in the ex vivo spectra can be seen. Figure 7c shows the average in vivo and ex vivo Raman spectra associated with the base prostate region. In general, all spectra acquired *in vivo* express peaks in the same 14 spectral bands as those on *ex vivo* spectra (see Table 4 for peak/molecular identification). Direct visual comparison between mean *in vivo* and *ex vivo* spectra for the base region of the prostate demonstrate they are similar in the fingerprint region based the bands/peaks that are expressed as well as their relative intensities. However, the peaks in the high wavenumber region however have noticeably lower intensities for *in vivo* data when compared to *ex vivo* data.

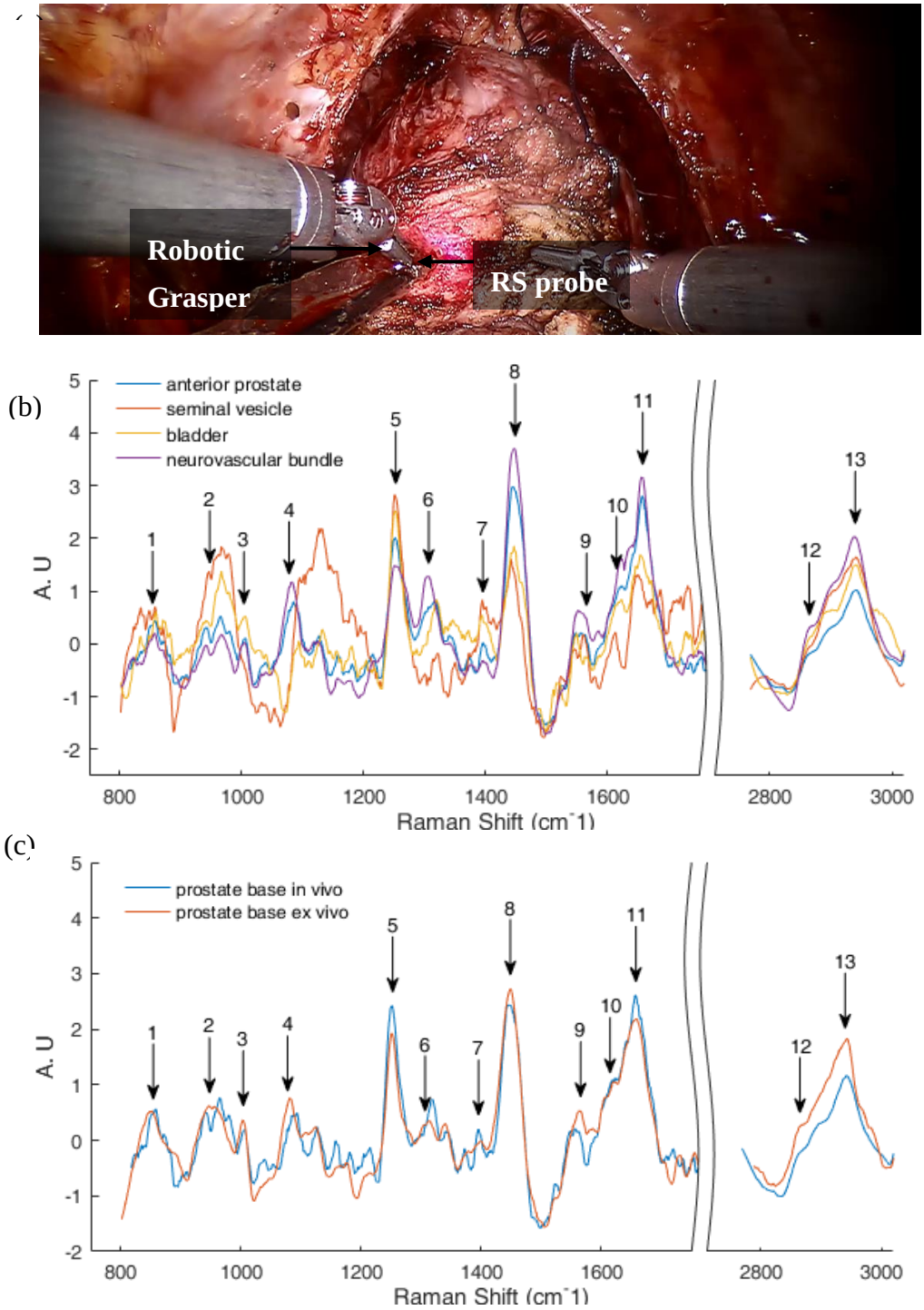

Figure 7 : (a) Close up views of Raman spectroscopy probe during spectral acquisition on prostate base *in vivo*. (b) Mean spectra of specific tissue classes acquired *in vivo*. (c) Comparison of average *in vivo* and *ex vivo* spectra for the base prostate region.

4.5 Discussion

There is a clinical need in oncology for new technologies to allow accurate and rapid intraoperative molecular tissue characterization at the surgical margin during tumor resection interventions. Optimal disease management using surgery is critical for prostate cancer patients where positive surgical margins occur for as many as 1 in 5 radical prostatectomy cases[5]. Limiting the risk of disease recurrence for patients undergoing radical prostatectomy can be achieved by ensuring the prostate organ is completely removed and that the disease has not spread beyond the prostatic capsule. Ensuring that no prostate tissue is left in the cavity following the procedure can also help minimize false positives during post-surgical follow-ups based on PSA, which is secreted by both normal and malignant prostate cells. Residual prostatic benign tissue can lead to detectable serum PSA which can be falsely interpreted at disease recurrence. The need to limit the resection of and damage to normal tissue is also critical in prostate cancer; for example, sparing nerves is critical to reduce the risk of erectile dysfunction and preserving continence[6], [48]. However, current standard of care technologies used to assist radical prostatectomy procedures are limited in their ability to provide detailed point-by-point molecular tissue characterization and thus cannot provide surgeons with the information they need to achieve optimal surgical outcome.

A growing number of radical prostatectomy procedures are performed worldwide using robotic-assisted surgical systems[41]. This rise in robotic-assisted procedures provides a unique opportunity for the mechanical integration of new tissue characterisation tools alongside standard robotic accessories (*e.g.* graspers, needle drivers, cauterizers) for routine intraoperative use. These new tools could then be used to address the current needs in prostate surgery, namely: i) prostate tissue detection, ii) nerve sparring and iii) detection of cancer cells that have invaded beyond the confines of the prostate. The use of optical technologies such as Raman spectroscopy can provide an avenue for point-by-point molecular tissue characterization and highly accurate classification as demonstrated over the last decades by several groups[35], [49]. Given sufficiently large datasets (spectra and tissue class labels determined based on histopathology analyses), mathematical models can be trained using supervised learning techniques for live tissue classification.

In this work, we have presented the integration of Raman spectroscopy to a robotic-assisted surgical system. Specifically, we have presented the initial steps that led to the use of the spectroscopy platform for *ex vivo* tissue characterization as well as a feasibility study demonstrating – for the first time – measurements of Raman spectra *in vivo* at the surgical margin during robotic-assisted radical prostatectomy procedures. Validation of the spectroscopy system's ability to acquire spectra at multiple angles compatible with those required for prostate measurements was assessed using a custom prostate-simulating phantom. Then, a preliminary clinical proof-of-principle study was presented based on *ex vivo* measurements. Using data acquired from 20 prostates (599 spectra in total), a classification model was produced based on support vector machines to distinguish prostate from extra prostatic tissue. Using a holdout validation dataset (25% of all spectra), the model was able to distinguish between prostatic and extra prostatic tissue with an accuracy of 91%, a sensitivity of 90.5% and specificity of 96%.

Although those preliminary results are promising, the development of sufficiently general models for live and reliable intraoperative tissue characterization will not only require larger datasets but also the development of modeling approaches that can perform independently of whether the measurements are made under *ex vivo* or *in vivo* conditions. As a first step in that direction, in this work we have demonstrated the feasibility of acquiring Raman spectra *in vivo* using a robotic-assisted surgical system and demonstrated the validity of the acquired spectra based on the detection of expected molecular vibrational modes in biological tissues as assessed by the presence of the main tissue bands and peaks (*e.g.*, amide bands, phenylalanine peak). As a preliminary demonstration of the consistency between *in vivo* and *ex vivo* measurements, *in vivo* and *ex vivo* spectra from the base region of prostate were compared and demonstrated to be compatible in the fingerprint region but significant relative intensity differences in the high wavenumber region were observed. Developing a classifier that is valid for clinical use will require either the demonstration of interchangeability between the two datasets or collection of enough *in vivo* spectra to train a robust classifier.

Robotic integration was sufficient for this proof of concept though many improvements remain possible. Firstly, spectral acquisitions were all dependent on the presence of an operator for the Raman spectroscopy system. Optimal integration of such a system will instead be controlled

by the pedals and switches provided directly to the surgeon through the da Vinci surgeon console (as is the case for existing activated instruments such as cauterizing ones). Moreover, the current "drop in" design requires the optical probe to be grasped by a separate instrument. Development of a custom robotic arm already integrated with the fibers, lenses and filters required for Raman spectroscopy will allow for more seamless spectral acquisitions. The integrative work outlined above however lays the groundwork for further study into characterization of prostate tissue at the surgical margin using Raman spectroscopy and similar optical techniques. Data gathering at a larger scale will be a crucial step towards the development of clinically relevant and robust algorithms capable of providing surgeons with information regarding tissue make up in real time. This technology holds promise for detecting prostate tissue left behind at the margin leading to more complete but circumscribed resections, of localizing cancer's spread when it extends out of the prostate and perhaps even of detecting nerves critical for erectile and urinary functions.

4.6 Conclusion

There is a strong clinical need for characterization of tissue (be it benign or cancerous) at the surgical margin during radical prostatectomy. The molecular specificity provided by Raman spectroscopy could be leveraged to achieve this goal given the right steps towards clinical translation. Here, for the first time, we've designed, built and integrated a Raman spectroscopy system to a surgical robotics platform and demonstrated the feasibility of acquiring measurements *in vivo* in real-time during RP (n=5). The same system was used on *ex vivo* human prostates (n=20) immediately following RP as a proof of concept that Raman spectroscopy can successfully be used to distinguish prostate tissue from surrounding organs and tissues with high accuracy.

4.7 Disclosures

F.Leblond is co-founder of ODS Medical Inc., a medical device company that seeks to commercialize the Raman spectroscopy system for real-time detection of tissue abnormalities.

4.8 Acknowledgments

This work was supported by a MEDTEQ/NSERC-CRD grant to F. Lesage and D. Trudel. The authors would like to thank Ian McDowall at Intuitive Surgical for providing parts and technical guidance; Sylvie Lau from Minogue Medical for providing invaluable training and technical assistance. Claudia Syed and Mirela Birlea for patient recruitment and technical support; Khaled Ajib for operating the da Vinci robot during phantom experiments. Rajeev Yadav from ODS Medical for technical guidance in spectral processing.

CHAPTER 5 GENERAL DISCUSSION

The general objective of this thesis was to demonstrate that a tissue characterization system using RS can be integrated into the da Vinci surgical platform for RA-RP to characterize tissue composition at the surgical margin during RA-RP. The following section will review the accomplishments with regards to the objectives laid out earlier and critically discuss each one.

The first objective set out in this work was the integration of an RS system to the da Vinci surgical robotics platform. We have successfully designed an RS system adapted for use in surgical robotics and elaborated a workflow compatible with its use clinically *in vivo*. The system performs RS at two excitation wavelengths through a single excitation fiber providing spectra in both the fingerprint and high wavenumber spectral regions. Integration with the da Vinci surgical platform is mainly accomplished through an adapted probe design which allows it to be inserted through a laparoscopic port and grasped by standard robotic grasping instruments. Once the probe is inserted and the system ready, the surgeon coordinates with the RS system operator to perform spectral measurements. Though this integration is functional, it leaves much room for improvement. Surgical robotics offer a platform where technological integration is made easy. Much like an iPhone provides developers with sensors, GUI elements, screen space, a camera, and interaction paradigms, the da Vinci platform offers a screen on which information can be overlayed, centralized controls to manipulate instruments, configurable pedals to toggle between instruments or trigger certain functions and more. The current implementation of the RS system to the robot fails to optimally take advantage of these features. Most notably, there lacks communication between the RS acquisition software and the surgeon/surgical robotics platform. For example, pedal based control of RS acquisitions would allow the surgeon to perform spectral acquisitions independently rather than providing verbal cues to a system operator. Information on the acquired spectra could be displayed to the surgeon directly in his console. It is worth noting that efforts were made in this direction in the scope of this project. A custom protocol was developed for communication and control of the RS acquisition software. A TCP/IP server was added to the acquisition software with a simple protocol allowing external platforms to trigger Raman acquisitions while setting certain parameters and obtaining information back from the system.

Automated power/exposure control algorithms (for both excitation wavelengths) allow for optimal power to be used for each spectral acquisition without the need for manual intervention. Integration of RS to the da Vinci platform could also use some improvement on the mechanical side of things. The current probe design uses 6 parallel smooth faces (much like an Allen key) to allow for grasping by a robotic clamp. The metal to metal contact between the graspers and the probe is slippery and causes the probe to rotate at extreme angles. This was remedied in our case by coating the probe with a sterile flexible plastic film before use (Tegaderm) though a more permanent solution such as knurling of the metal faces would be more ideal.

The second objective set out in this project was the collection of ex vivo and in vivo Raman spectra from human prostate and peri prostatic organs. The first subobjective here was to collect Raman spectra from whole, unprocessed prostates immediately following RP with the objective of characterising Raman spectra in different prostatic regions. To do this, a protocol was developed wherein the prostate was divided into 5 sub regions (the apex, the base, the 2 lateral lobes, and the posterior face). 5 acquisitions were performed for each region on 20 whole human prostates in the operating room immediately following RP. When possible, measurements were made on extra-prostatic tissue available (vas deferens, seminal vesicles). Following this protocol, we successfully acquired ~600 spectra on whole human prostate. These spectra serve as the basis for a proof of concept that RS can be used to successfully characterize prostate tissue and differentiate between prostatic and extra prostatic tissue discussed further. Distinguishing between prostatic and prostatic tissue has clinical relevance though it is only a part of the puzzle. Being able to distinguish between cancerous prostate tissue and benign prostate tissue at the margin in real time would also have great clinical value. The current protocol is not suited to detect cancer as it finds ground truth only in visual segmentation of the prostate into gross anatomical region. Pushing this research farther will require the introduction of more detailed tissue analysis at spots interrogated for RS (eg. By co-registration with Histopathology) for use as ground truth. The second subobjective set out in this project was the collection of Raman spectra from prostate and peri-prostatic organs in vivo to assess the feasibility of distinguishing between prostatic and peri-prostatic tissue intra operatively. Using the previously described system in combination with a da Vinci surgical robot we have successfully acquired ~20 Raman spectra in vivo during RA-RP from 4 patients. To our knowledge, this is a

world first. Though we have shown the feasibility of acquiring RS spectra in vivo, we have insufficient data to determine whether or not these spectra can be used to distinguish between prostatic and peri prostatic tissue successfully. It also remains to be answered whether spectra acquired ex vivo can be used to train models for classification in vivo and vice versa. Answering these questions will require acquisition of larger datasets. This rationale lead to the addition of the third sub-objective in this category: automating the process of acquiring Raman spectra from prostate specimens. Through a collaboration with fourth year engineering students, we successfully developed an automated platform capable of acquiring Raman spectra from a flat sample. The platform is a highly modified 3D printer which cradles an optical probe and communicates with RS acquisition software to perform spectra on points preselected by an operator. Integration was successfully tested on 2 human prostate specimens. A typical prostate slice processed manually by one of our team members requires roughly an hour of work while the platform accomplishes the same results in roughly 20 minutes. Development of this platform is now underway to scale data collection across multiple sites with the industrial partners ODS Medical and Intuitive Surgical.

The final objective of this project was to use the acquired datasets from objective 2 to evaluate the potential of RS to provide clinically relevant tissue characterization. Consulting with the pathologist (DT) and surgeon (KZ) collaborating on this project, lead to the decision of classifying between prostatic and extra prostatic tissue. Spectra acquired from the apex, base, lateral lobes and posterior region of *ex vivo* human prostate were grouped under the label ‘prostate’ while those acquired on seminal vesicles and the vas deferens were grouped under the label ‘extra-prostatic’. We trained an SVM model with a quadratic kernel on this dataset using 25% holdout validation and obtained an accuracy of 91%, a sensitivity of 90.5% and specificity of 96%. These results, though preliminary, are promising and indicate Raman has potential as a classification tool in RP. Though promising, open questions remain on how these results will translate well *in vivo.* It remains to be shown that models trained *ex vivo* can be used to perform classifications on similar tissue *in vivo*. To assess performance of these methods *in vivo* will thus require collection of a large dataset *in vivo*. Classification performance on models trained on an *in vivo* dataset, models trained on an *ex vivo* dataset, and models trained on mixed *in vivo/ex vivo* datasets may then be assessed and compared. As a preliminary demonstration of the consistency between *in vivo* and *ex vivo*

measurements, *in vivo* and *ex vivo* spectra from the base region of prostate were compared and demonstrated to be compatible in the fingerprint region but significant relative intensity differences in the high wavenumber region were observed.

CHAPTER 6 CONCLUSION AND RECOMMENDATIONS

A pressing clinical need exists for tissue characterization of prostate tissue during RP : prostate tissue is difficult to distinguish from extra prostatic tissue due to the lack of a clear histo RS coupled with machine learning holds great potential as a solution to address this need through highly sensitive/specific molecular fingerprinting. This work has summarized the engineering, of an RS system adapted for use in RARP. A "drop-in" approach was used wherein a probe designed to be grasped by robotic grasping instruments is inserted to the patient through a standard laparoscopic port and manipulated by the surgeon. This system was used to demonstrate the ability to acquire Raman spectra on human prostate and surrounding organs *in vivo* for the first time on 5 patients. A proof of concept study was performed on *ex vivo* tissue, where it is more feasible to acquire large datasets, to assess the potential of RS to provide clinically relevant information in RA-RP. Roughly 600 spectra were collected from 20 whole human prostates *ex vivo* immediately following resection. Spectra were grouped as either prostatic or extra prostatic tissue and SVM based machine learning techniques (quadratic SVM, 25% holdout validation) demonstrated RS's ability to differentiate between prostatic and extra-prostatic tissue with accuracy, sensitivity & specificity > 90%. The challenges associated with scaling data collection also lead to the development of an automated RS platform which was presented in this work.

This study holds a few significant limitations. Most notably, the proof of concept addressed the need for prostate tissue identification but did not address the need for cancer detection at the margin. Our group has demonstrated intracapsular detection with high accuracy but the translation of this work to extracapsular detection poses a significant challenge – cancer at the margin is relatively rare (1 in 5 cases) and when it is present it is sparse. Pinpointing the spots to interrogate and developing a strategy to correlate them with histopathology will therefore be an important challenge. Furthermore, research will be required before the technology is mature enough for *in vivo* diagnostic use. Notably, the next logical step will be to acquire far larger datasets both *ex vivo* and *in vivo* in order to reproduce the preliminary results presented here at scale and test the hypothesis that Raman spectra acquired *ex vivo* and *in vivo* can be used interchangeably to train

classifiers. Finally the robotic integration using a drop-in approach, though functional, hampers the clinical workflow in ways that could be avoided with the design of a specialized robotic arm.

All in all, this work is a promising step forward paving the way for future clinical applications of RS *in vivo*. The proof of concept in this work focused on the detection of prostate tissue though the methods presented here are valid for any context where molecular fingerprinting can provide useful diagnostic information.

BIBLIOGRAPHY

[1] S. BW and W. CP, *World Cancer Report 2014.* .

[2] R. L. Siegel, K. D. Miller, and A. Jemal, "Cancer statistics, 2015," *CA Cancer J Clin*, vol. 65, no. 1, pp. 5–29, Feb. 2015.

[3] M. Akand, O. Celik, E. Avci, I. Duman, and T. Erdogru, "Open, laparoscopic and robot-assisted laparoscopic radical prostatectomy: comparative analysis of operative and pathologic outcomes for three techniques with a single surgeon's experience," *Eur Rev Med Pharmacol Sci*, vol. 19, no. 4, pp. 525–531, Feb. 2015.

[4] A. Y. Odisho, S. L. Washington, M. V. Meng, J. E. Cowan, J. P. Simko, and P. R. Carroll, "Benign Prostate Glandular Tissue at Radical Prostatectomy Surgical Margins," *Urology*, vol. 82, no. 1, pp. 154–159, Jul. 2013.

[5] P. H. Tan *et al.*, "International Society of Urological Pathology (ISUP) Consensus Conference on Handling and Staging of Radical Prostatectomy Specimens. Working group 5: surgical margins," *Mod. Pathol.*, vol. 24, no. 1, pp. 48–57, Jan. 2011.

[6] A. Briganti *et al.*, "Predicting erectile function recovery after bilateral nerve sparing radical prostatectomy: a proposal of a novel preoperative risk stratification," *J Sex Med*, vol. 7, no. 7, pp. 2521–2531, Jul. 2010.

[7] A. Goyette *et al.*, "Sub-diffuse interstitial optical tomography to improve the safety of brain needle biopsies: a proof-of-concept study," *Opt Lett*, vol. 40, no. 2, pp. 170–173, Jan. 2015.

[8] C. Kallaway *et al.*, "Advances in the clinical application of Raman spectroscopy for cancer diagnostics," *Photodiagnosis Photodyn Ther*, vol. 10, no. 3, pp. 207–219, Sep. 2013.

[9] A. Smekal, "Zur Quantentheorie der Dispersion," *Naturwissenschaften*, vol. 11, pp. 873–875, Oct. 1923.

[10] M. Jermyn *et al.*, "Intraoperative brain cancer detection with Raman spectroscopy in humans," *Sci Transl Med*, vol. 7, no. 274, p. 274ra19, Feb. 2015.

[11] "Introduction, Basic Theory and Principles," in *Modern Raman Spectroscopy – A Practical Approach*, Wiley-Blackwell, 2005, pp. 1–21.

[12] C. V. Raman and K. S. Krishnan, "A New Type of Secondary Radiation," *Nature*, vol. 121, no. 3048, pp. 501–502, Mar. 1928.

[13] J. Zhao, H. Lui, D. I. McLean, and H. Zeng, “Automated autofluorescence background subtraction algorithm for biomedical Raman spectroscopy,” *Appl Spectrosc*, vol. 61, no. 11, pp. 1225–1232, Nov. 2007.

[14] “The Raman Experiment – Raman Instrumentation, Sample Presentation, Data Handling and Practical Aspects of Interpretation,” in *Modern Raman Spectroscopy – A Practical Approach*, Wiley-Blackwell, 2005, pp. 23–70.

[15] M. Jermyn *et al.*, “A review of Raman spectroscopy advances with an emphasis on clinical translation challenges in oncology,” *Phys Med Biol*, vol. 61, no. 23, pp. R370–R400, 07 2016.

[16] C. Beleites, U. Neugebauer, T. Bocklitz, C. Krafft, and J. Popp, “Sample Size Planning for Classification Models,” *Analytica Chimica Acta*, vol. 760, pp. 25–33, Jan. 2013.

[17] E. Guevara, *vancouver: Implementation of the Vancouver Raman Algorithm. Reference: Zhao, J., Lui, H., McLean, D. I., & Zeng, H. (2007). Automated Autofluorescence Background Subtraction Algorithm for B.*. 2016.

[18] T. Randolph, “Scale-based normalization of spectral data.” University of washington - department of biostatistics, 2005.

[19] S. J. Choquette, E. S. Etz, W. S. Hurst, D. H. Blackburn, and S. D. Leigh, “Relative intensity correction of Raman spectrometers: NIST SRMs 2241 through 2243 for 785 nm, 532 nm, and 488 nm/514.5 nm excitation,” *Appl Spectrosc*, vol. 61, no. 2, pp. 117–129, Feb. 2007.

[20] M. G. Madden and A. G. Ryder, “Machine learning methods for quantitative analysis of Raman spectroscopy data,” in *Opto-Ireland 2002: Optics and Photonics Technologies and Applications*, 2003, vol. 4876, pp. 1130–1140.

[21] W. Fu and W. S. Hopkins, “Applying Machine Learning to Vibrational Spectroscopy,” *J. Phys. Chem. A*, vol. 122, no. 1, pp. 167–171, Jan. 2018.

[22] E. Ryzhikova *et al.*, “Raman spectroscopy of blood serum for Alzheimer’s disease diagnostics: specificity relative to other types of dementia,” *J Biophotonics*, vol. 8, no. 7, pp. 584–596, Jul. 2015.

[23] E. Cinotti *et al.*, “Optical diagnosis of a metabolic disease: cystinosis,” *J Biomed Opt*, vol. 18, no. 4, p. 046013, Apr. 2013.

[24] K. L. Cloyd *et al.*, “Characterization of Porcine Aortic Valvular Interstitial Cell ‘Calcified’ Nodules,” *PLOS ONE*, vol. 7, no. 10, p. e48154, Oct. 2012.

[25] A. Y. F. You *et al.*, “Raman spectroscopy imaging reveals interplay between atherosclerosis and medial calcification in the human aorta,” *Science Advances*, vol. 3, no. 12, p. e1701156, Dec. 2017.

[26] R. E. Kast, S. C. Tucker, K. Killian, M. Trexler, K. V. Honn, and G. W. Auner, “Emerging technology: applications of Raman spectroscopy for prostate cancer,” *Cancer Metastasis Rev.*, vol. 33, no. 2–3, pp. 673–693, Sep. 2014.

[27] P. Crow, A. Ritchie, M. Wright, C. Kendall, and N. Stone, “Evaluation of Raman spectroscopy to provide a real time, optical method for discrimination between normal and abnormal tissue in the prostate,” *European Urology Supplements*, vol. 1, no. 1, p. 92, Jan. 2002.

[28] P. Crow *et al.*, “The use of Raman spectroscopy to identify and grade prostatic adenocarcinoma in vitro,” *Br. J. Cancer*, vol. 89, no. 1, pp. 106–108, Jul. 2003.

[29] P. Crow *et al.*, “The use of Raman spectroscopy to differentiate between different prostatic adenocarcinoma cell lines,” *Br J Cancer*, vol. 92, no. 12, pp. 2166–2170, Jun. 2005.

[30] L. Wang *et al.*, “Raman spectroscopy, a potential tool in diagnosis and prognosis of castration-resistant prostate cancer,” *J Biomed Opt*, vol. 18, no. 8, p. 87001, Aug. 2013.

[31] P. Crow, J. S. Uff, J. A. Farmer, M. P. Wright, and N. Stone, “The use of Raman spectroscopy to identify and characterize transitional cell carcinoma in vitro,” *BJU Int.*, vol. 93, no. 9, pp. 1232–1236, Jun. 2004.

[32] B. W. D. de Jong *et al.*, “Discrimination between Nontumor Bladder Tissue and Tumor by Raman Spectroscopy,” *Anal. Chem.*, vol. 78, no. 22, pp. 7761–7769, Nov. 2006.

[33] “Raman technologies in cancer diagnostics - Analyst (RSC Publishing).” [Online]. Available: http://pubs.rsc.org/en/content/articlelanding/2016/an/c5an01786f#!divAbstract. [Accessed: 31-Jul-2018].

[34] P. Crow, A. Molckovsky, N. Stone, J. Uff, B. Wilson, and L.-M. WongKeeSong, “Assessment of fiberoptic near-infrared raman spectroscopy for diagnosis of bladder and prostate cancer,” *Urology*, vol. 65, no. 6, pp. 1126–1130, Jun. 2005.

[35] H. Lui, J. Zhao, D. McLean, and H. Zeng, “Real-time Raman spectroscopy for in vivo skin cancer diagnosis,” *Cancer Res.*, vol. 72, no. 10, pp. 2491–2500, May 2012.

[36] R. O. P. Draga *et al.*, “In Vivo Bladder Cancer Diagnosis by High-Volume Raman Spectroscopy,” *Anal. Chem.*, vol. 82, no. 14, pp. 5993–5999, Jul. 2010.

[37] K. Aubertin *et al.*, “Mesoscopic characterization of prostate cancer using Raman spectroscopy: potential for diagnostics and therapeutics,” *BJU International*, vol. 0, no. 0.

[38] P. J. Gray, C. C. Lin, A. Jemal, and J. A. Efstathiou, “Recent trends in the management of localized prostate cancer: Results from the National Cancer Data Base.,” *JCO*, vol. 32, no. 15_suppl, pp. 5066–5066, May 2014.

[39] J. Chen, C. Oromendia, J. A. Halpern, and K. V. Ballman, “National trends in management of localized prostate cancer: A population based analysis 2004-2013,” *Prostate*, vol. 78, no. 7, pp. 512–520, May 2018.

[40] E. P. Estey, “Robotic prostatectomy: The new standard of care or a marketing success?,” *Can Urol Assoc J*, vol. 3, no. 6, pp. 488–490, Dec. 2009.

[41] S. L. Chang, A. S. Kibel, J. D. Brooks, and B. I. Chung, “The impact of robotic surgery on the surgical management of prostate cancer in the USA,” *BJU International*, vol. 115, no. 6, pp. 929–936.

[42] M. Jermyn *et al.*, “Highly Accurate Detection of Cancer In Situ with Intraoperative, Label-Free, Multimodal Optical Spectroscopy,” *Cancer Res.*, vol. 77, no. 14, pp. 3942–3950, 15 2017.

[43] J. Desroches *et al.*, “A new method using Raman spectroscopy for in vivo targeted brain cancer tissue biopsy,” *Scientific Reports*, vol. 8, no. 1, p. 1792, Jan. 2018.

[44] *ASTM International - Standard References for ASTM E2911 - 13*. .

[45] “McCreery Group | Raman Materials.” [Online]. Available: http://www.chem.ualberta.ca/~mccreery/ramanmaterials.html#acetamidophenol. [Accessed: 24-Jul-2018].

[46] K. Aubertin *et al.*, “Raman spectroscopy for prostate cancer characterization: potential for precision diagnostics and therapeutics,” *British Journal of Urology International*, Mar. 2018.

[47] J.-U. Stolzenburg and M. C. Truss, “Technique of laparoscopic (endoscopic) radical prostatectomy,” *BJU International*, vol. 91, no. 8, pp. 749–757.

[48] N. Suardi *et al.*, “Nerve-sparing approach during radical prostatectomy is strongly associated with the rate of postoperative urinary continence recovery,” *BJU Int.*, vol. 111, no. 5, pp. 717–722, May 2013.

[49] M. A. Short, S. Lam, A. McWilliams, J. Zhao, H. Lui, and H. Zeng, “Development and preliminary results of an endoscopic Raman probe for potential in vivo diagnosis of lung cancers,” *Opt Lett*, vol. 33, no. 7, pp. 711–713, Apr. 2008.